11-15-2018

Distinct Proteostasis Circuits Cooperate in Nuclear and Cytoplasmic Protein Quality Control

Rahul S. Samant

Christine M. Livingston

Emily M. Sontag

Judith Frydman

Nature, Vol. 563 (November 15, 2018): 407-411. DOI.

Distinct Proteostasis Circuits Cooperate in Nuclear and Cytoplasmic Protein Quality Control

Rahul S. Samant
Department of Biology, Stanford University, Stanford, CA
Christine M. Livingston
Present address: Janssen Research and Development, Spring House, PA
Department of Biology, Stanford University, Stanford, CA
Emily M. Sontag
Department of Biology, Stanford University, Stanford, CA
Judith Frydman
Department of Biology, Stanford University, Stanford, CA
Department of Genetics, Stanford University, Stanford, CA

Abstract

Protein misfolding is linked to a wide array of human disorders, including Alzheimer's disease, Parkinson's disease and type II diabetes[1,2]. Protective cellular protein quality control (PQC) mechanisms have evolved to selectively recognize misfolded proteins and limit their toxic effects[3,4,5,6,7,8,9], thus contributing to the maintenance of the proteome (proteostasis). Here we examine how molecular chaperones and the ubiquitin–proteasome system cooperate to recognize and promote the clearance of soluble misfolded proteins. Using a panel of PQC substrates with distinct characteristics and localizations, we define distinct chaperone and ubiquitination circuitries that execute quality control in the cytoplasm and nucleus. In the cytoplasm, proteasomal degradation of misfolded proteins requires tagging with mixed lysine 48 (K48)- and lysine 11 (K11)-linked ubiquitin chains. A distinct combination of E3 ubiquitin ligases and specific chaperones is required to achieve each type of linkage-specific ubiquitination. In the nucleus, however, proteasomal degradation of misfolded proteins requires only K48-linked ubiquitin chains, and is thus independent of K11-specific ligases and chaperones. The distinct ubiquitin codes for nuclear and cytoplasmic PQC appear to be linked to the function of the ubiquilin protein Dsk2, which is specifically required to clear nuclear misfolded proteins. Our work defines the principles of cytoplasmic and nuclear PQC as distinct, involving combinatorial recognition by defined sets of cooperating chaperones and E3 ligases. A better understanding of how these organelle-specific PQC requirements implement proteome integrity has implications for our understanding of diseases linked to impaired protein clearance and proteostasis dysfunction.

Main

Misfolded proteins, arising during biogenesis or through proteotoxic damage, are highly toxic; they accumulate in distinct regions (puncta) within cells[6,7,8,9] and form aggregates that are associated with neurodegenerative diseases[1]. Misfolded proteins must be cleared: the process involves the cooperation of chaperones and components of the ubiquitin–proteasome system (UPS)[3,4,5] (Fig. 1a), but is poorly understood.

Fig. 1: Combined deletion of certain E3 ligases impairs the clearance of misfolded proteins.

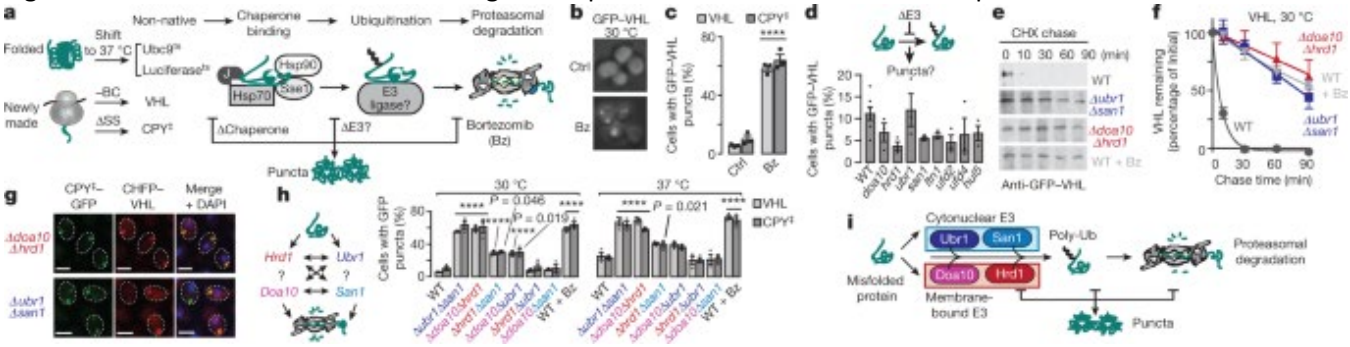

a, Proteins can become misfolded for different reasons; in our experiments (involving non-native proteins), the temperature-sensitive proteins Ubc9^{ts} or luciferase^{ts} misfold at temperatures of 37 °C; VHL misfolds in the absence of elongin BC (BC); and CPY‡ misfolds because it lacks its signal sequence (SS). Conserved pathways dispose of these aberrant proteins, with initial recognition by chaperones of the Hsp70 and Hsp90 families, J-domain proteins and Sse1; ubiquitination by one or more E3 ligases; and targeting for proteasomal degradation. Blocking any step (for instance, with the proteasome inhibitor bortezomib (Bz) or by omitting E3s or chaperones) triggers the sequestration of misfolded proteins into puncta. **b**, **c**, VHL and CPY‡ form puncta upon proteasome inhibition. Wild-type cells expressing galactose-inducible GFP–VHL or CPY‡–GFP were shifted to glucose media with 50 μM Bz or vehicle control (Ctrl) for 1 h to shut off expression. Fixed cells were imaged by fluorescence microscopy. **c**, Percentage of cells with GFP–VHL puncta. **d**, Deleting individual E3s implicated in PQC does not increase puncta formation. Experiment performed as in panel **b**, but using strains with endogenous deletions of E3s. WT, wild type. **e**, **f**, Misfolded proteins are stabilized in *Δubr1Δsan1* and *Δdoa10Δhrd1* strains: **e**,

cycloheximide (CHX) chase and immunoblot were used to assess the stability of GFP–VHL in E3 double-deletion strains, or following 50 μM Bz treatment; **f**, densitometric quantification of bands relative to $t = 0$ (mean ± s.e.m. from three biologically independent experiments). **g**, Multiple misfolded proteins are sequestered in the same subcellular location. Experiment performed as in panel **b**, but in strains co-expressing VHL with CPY‡. Images represent more than 100 cells from each of three biologically independent experiments. Scale bars represent 2 μm. **h**, Deleting certain E3 pairs increases puncta formation. Experiment performed as in panel **b**, but using strains with endogenous deletions of E3 pairs. On the right, cells were shifted to 37 °C for the shut-off. **i**, Clearance of misfolded proteins requires a soluble E3, Ubr1 or San1, and a membrane-bound E3, Doa10 or Hrd1. **c**, **d**, **h**, 300 cells were counted per condition. Bars represent mean ± s.e.m. from three biologically independent experiments, except for the wild type in panel **d** (seven biologically independent experiments). Statistically significant differences versus wild type, calculated by two-tailed Student's *t*-test (**c**), or one-way analysis of variance (ANOVA) plus Dunnett's multiple comparisons test (**d**, **h**), are indicated with the adjusted *P* value, or with **** for $P < 0.0001$.

To better understand the PQC of soluble proteins, we used a panel of substrates that reflects different types of misfolding, including two temperature-sensitive proteins (Ubc9^{ts} and luciferase^{ts}), a protein (the Von Hippel–Lindau tumour suppressor, VHL) that cannot fold without its oligomeric partners elongin B and C, and translocation-defective carboxypeptidase yscY (CPY*) that lacks its signal sequence (CPY‡)[6,7,9,10]. We found that terminally misfolded VHL or CPY‡ conjugated to green fluorescent protein (GFP) was cleared within 1 hour, with only around 10% of cells containing GFP-positive puncta (Fig. 1b, c). Blocking proteasomal degradation with the proteasome inhibitor bortezomib led to the accumulation of these proteins in GFP-positive puncta. Temperature-sensitive proteins, such as Ubc9^{ts}–GFP, are diffuse when folded at 30 °C, but upon misfolding at 37 °C are also degraded through the proteasome or accumulate in puncta (Extended Data Fig. 1a)[6,7]. Of note, native wild-type Ubc9 is soluble at either temperature.

To identify the E3 ubiquitin (Ub) ligases involved in PQC, we expressed GFP–VHL in a library of 41 *Saccharomyces cerevisiae* single-deletion strains comprising most non-essential E3 ubiquitin ligases (Extended Data Fig. 1b), including E3s that have previously been implicated in PQC (Fig. 1d). No single deletion caused a notable increase in puncta formation compared with wild-type cells, suggesting that no single E3 is essential for PQC of this substrate.

Given that E3 ligases can have redundant functions[11], we next deleted pairs of E3s previously implicated in PQC. The cytoplasmic E3 Ubr1 and the nuclear E3 San1 cooperate in the clearance of some cytoplasmic proteins[11,12]. The E3s Hrd1, which is anchored in the endoplasmic reticulum (ER) membrane, and Doa10, also localized to the ER and to the inner nuclear membrane[13], trigger ER-associated protein degradation (ERAD)[14]. We found that both *Δubr1Δsan1* and *Δdoa10Δhrd1* strains abrogated the degradation of all PQC substrates to the same extent as proteasome inhibition (see, for example, the results of cycloheximide chase in Fig. 1e, f and Extended Data Fig. 1c). Notably, all PQC substrates accumulated in the same puncta in these strains (Fig. 1g and Extended Data Fig. 1d). Therefore, multiple misfolded proteins use the same E3 systems for proteasomal degradation, and are sequestered together in the same PQC compartments in the absence of these E3 systems.

To determine why the deletion of either E3 pair stabilized our PQC substrates similarly, we tested the effect of doubly deleting all possible combinations of these four E3 ligases—Ubr1, San1, Doa10 and Hrd1 (Fig. 1h and Extended Data Fig. 1e). Puncta formation and cycloheximide chase assays showed that only specific combinations of deletions abrogate clearance. Strong stabilization was observed in *Δubr1Δsan1* and *Δdoa10Δhrd1* strains. A moderate effect was found with *Δdoa10Δubr1* and *Δhrd1Δsan1*. Strikingly, *Δdoa10Δsan1* and *Δhrd1Δubr1* had no effect on PQC, suggesting that these pairs of ligases—Doa10/San1 and Hrd1/Ubr1—provide parallel, optimal combinations for PQC clearance. This E3 circuit logic appeared to be general, as it operated for all substrates tested at 30 °C and 37 °C. Thus PQC clearance requires

parallel pathways of specific pairs of E3 ligases, combining one of the soluble E3s (either Ubr1 or San1; blue in Fig. 1i) and one of the membrane-bound E3s (either Doa10 or Hrd1; red). Overexpressing an E3 in any of the double-deletion strains rescued clearance only in those strains deleted for that particular E3 (Extended Data Fig. 1f). Therefore, E3 function is not interchangeable, even at higher expression levels, and PQC requires specific E3 combinations. The functional cooperation between E3 ligases may involve a physical complex, as immunoprecipitation experiments show that San1 associates with Doa10 but not with Hrd1 (Extended Data Fig. 2). We were unable to co-immunoprecipitate Ubr1 with Hrd1 (or Doa10), so these ligases may bind transiently, or cooperate functionally through separate complexes.

To examine whether the PQC defects observed above were linked to impaired ubiquitination, we expressed a terminally misfolded Flag-tagged VHL mutant (L158P; ref. 10) in either wild-type cells or the panel of double E3 deletions. VHL was immunoprecipitated under harsh denaturing conditions, followed by anti-ubiquitin immunoblot detection (Fig. 2a). In wild-type cells, polyubiquitin chains were clearly attached to VHL. In the *Δubr1Δsan1* and *Δdoa10Δhrd1* cells, VHL ubiquitination was markedly reduced, indicating that these E3 pairs promote VHL clearance through ubiquitination. No clear differences in VHL ubiquitination were observed in any other strains. A similar strategy examined how E3 deletions specifically affect VHL tagging with a canonical proteasomal signal, K48-linked Ub (in which the lysine 48 residue of one ubiquitin molecule is joined to the carboxyl terminus of the next ubiquitin in the chain, and so on) (Fig. 2b)[5]. Surprisingly, K48-linked VHL ubiquitination was strongly reduced in *Δubr1Δsan1* but not in *Δdoa10Δhrd1* cells. Conversely, the alternative proteasome-targeting signal, K11-linked Ub[5,15,16,17,18], was unaffected in *Δubr1Δsan1* cells but was abrogated in *Δdoa10Δhrd1* cells. Note that misfolded VHL was ubiquitinated with both K48-linked and K11-linked ubiquitin chains in wild-type cells. A quantitative ubiquitin-linkage-specific ELISA assay for K11- or K48-linked chains confirmed that Ubr1 and San1 mediate VHL tagging with K48–Ub chains, whereas Doa10 and Hrd1 promote K11-linked ubiquitination (Extended Data Fig. 3a, b). Upon proteasome inhibition, the VHL puncta co-localized with both K11- and K48-linked ubiquitin (Fig. 2c), supporting the conclusion that VHL itself is modified with ubiquitin chains containing both K48 and K11 linkages.

Fig. 2: Cytoplasmic misfolded proteins are modified with both K11- and K48- linked ubiquitin chains.

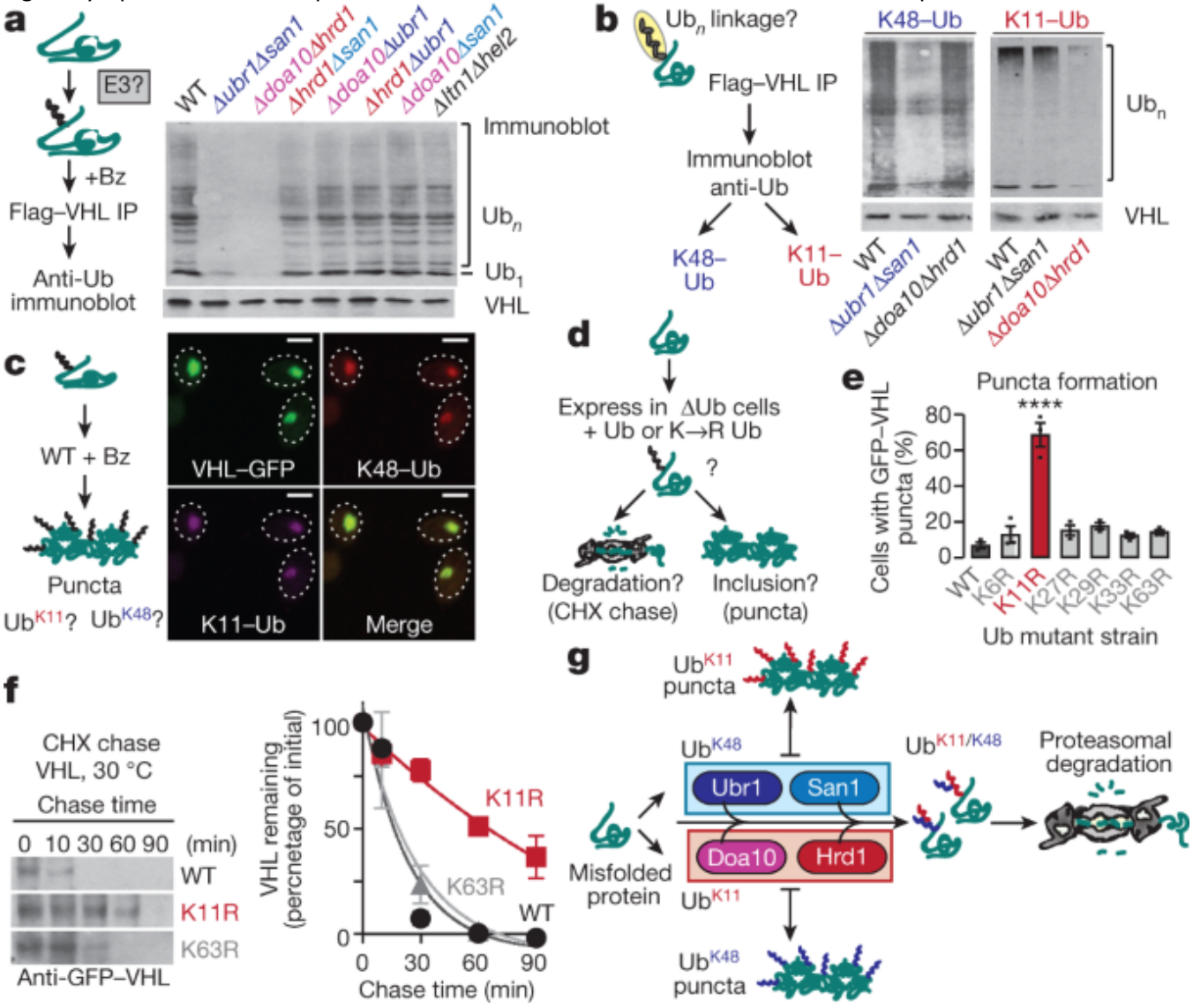

a, VHL ubiquitination is impaired in *Δubr1Δsan1* and *Δdoa10Δhrd1* strains. Denaturing immunoprecipitation (IP) for Flag–VHL was followed by immunoblot for ubiquitin in WT or E3 double-deletion strains. Deletion of the co-translational E3s Ltn1 and Hel2 served as a control. **b**, K48–Ub and K11–Ub linkages are reduced on Flag–VHL in *Δubr1Δsan1* and *Δdoa10Δhrd1* strains, respectively. Experiment performed as in panel **a**, but using K48–Ub or K11–Ub specific antibodies for immunoblot. **c**, K48–Ub and K11–Ub co-localize with GFP–VHL puncta. Experiment performed as in Fig. 1b. Fixed cells were spheroplasted and immunostained before imaging by confocal fluorescence microscopy. Images represent more than 100 cells from each of three independent experiments. Scale bars represent 2 μm. **d–f**, VHL clearance is impaired in the absence of K11–Ub linkages. **d**, Cells co-expressing galactose-inducible GFP–VHL, with either WT or K-to-R mutant Ub as their only ubiquitin source, were shifted to glucose media for 1 h to shut off expression. 300 cells were counted per condition. **e**, Percentage of cells with GFP–VHL puncta (mean ± s.e.m. from three biologically independent experiments). Only Ub^{K11R} significantly altered the percentage of puncta-positive cells versus WT (one-way ANOVA plus Dunnett's multiple comparisons test; ****$P < 0.0001$). **f**, CHX chase and immunoblot to assess GFP–VHL stability in Ub mutant strains. Graphs represent densitometric quantification relative to $t = 0$ (mean ± s.e.m. from three biologically independent experiments). **g**, Doa10/Hrd1 and Ubr1/San1 E3 ligases collaborate to ubiquitinate misfolded proteins with branched K11/K48 chains, thereby targeting them for proteasomal clearance. Inhibition

of either type of linkage results in the sequestration of the misfolded proteins with only Ub^{K48} or Ub^{K11} into puncta. **a**, **b**, **f**, Immunoblots represent three biologically independent experiments.

We next examined PQC in cells expressing a single copy of ubiquitin that carries individual lysine to arginine (K-to-R) mutations, and is therefore unable to form specific linkages (Fig. 2d). Ub^{K48R} is lethal[19], and could not be tested. VHL was degraded in all other K-to-R variants except in Ub^{K11R} cells, where VHL clearance was impaired, leading to its accumulation in puncta (Fig. 2e, f). Importantly, K11–Ub linkages were not generally required for proteasomal clearance, given that the non-misfolded cytoplasmic substrates Ub-R-GFP and Ub^{G76V}–GFP were degraded normally in Ub^{K11R} cells (Extended Data Fig. 4). Consistent with our data implicating ER-resident E3 ligases in K11–Ub tagging of soluble PQC substrates, the Ub^{K11R} strain has been shown to be sensitive to ER stress[16].

We next examined whether misfolded VHL is tagged with mixed K48- and K11-linked ubiquitin chains. Sequential double immunoprecipitations first isolated Flag-tagged VHL and then isolated either K48- or K11-linked chains (Extended Data Fig. 5a). The presence of K11- or K48-linked chains in either flow-through or bound fractions was then detected by immunoblot. All of the K11- and K48-linked chains were present only in the bound fractions of each immunoprecipitate (Extended Data Fig. 5b), showing that misfolded VHL is tagged with both K11- and K48-linked ubiquitin chains. Additionally, an antibody that recognizes branched K11/K48 linkages, with K11- and K48-linked chains extending from the same ubiquitin molecule[18], reacted with misfolded VHL in both immunofluorescence and immunoprecipitation experiments (Extended Data Fig. 5c–e). Notably, reactivity with the branched K11/K48 antibody required the presence of both K48- and K11-specific E3 ligases (Extended Data Fig. 5e). We conclude that a dual ubiquitin code involving both K11 and K48 is required for clearance of soluble PQC substrates. K11 ubiquitination is mediated by either of the membrane-bound E3s, Doa10 or Hrd1, and K48 ubiquitination is mediated by either of the soluble E3s, Ubr1 or San1, thus explaining the requirement for pairs of E3 ligases for PQC clearance. Given that deletion of one E3 pair did not abrogate the action of the other, addition of K11- or K48-linked chains does not require a particular sequential order.

It is unclear how chaperone proteins—known to be key mediators of PQC[1,3,4]—facilitate ubiquitination and clearance. Chaperones could simply maintain the solubility of misfolded proteins, or they could specifically direct them along an E3 clearance pathway (Fig. 3a). We used the ubiquitin-linkage-specific ELISA assay to identify whether chaperones implicated in PQC are required to tag misfolded VHL with either K11–Ub or K48–Ub (Fig. 3b). We found that cells lacking Ssa1 and Ssa2—the major cytosolic proteins of the heat-shock protein (Hsp)70 family required for PQC clearance[7,10,20]—were strongly impaired in ubiquitination with either linkage. By contrast, the ribosome-associated Hsp70s Ssb1 and Ssb2 were dispensable for degradation[10] and ubiquitination.

Fig. 3: K11- and K48- linked ubiquitination of misfolded proteins involves different chaperones.

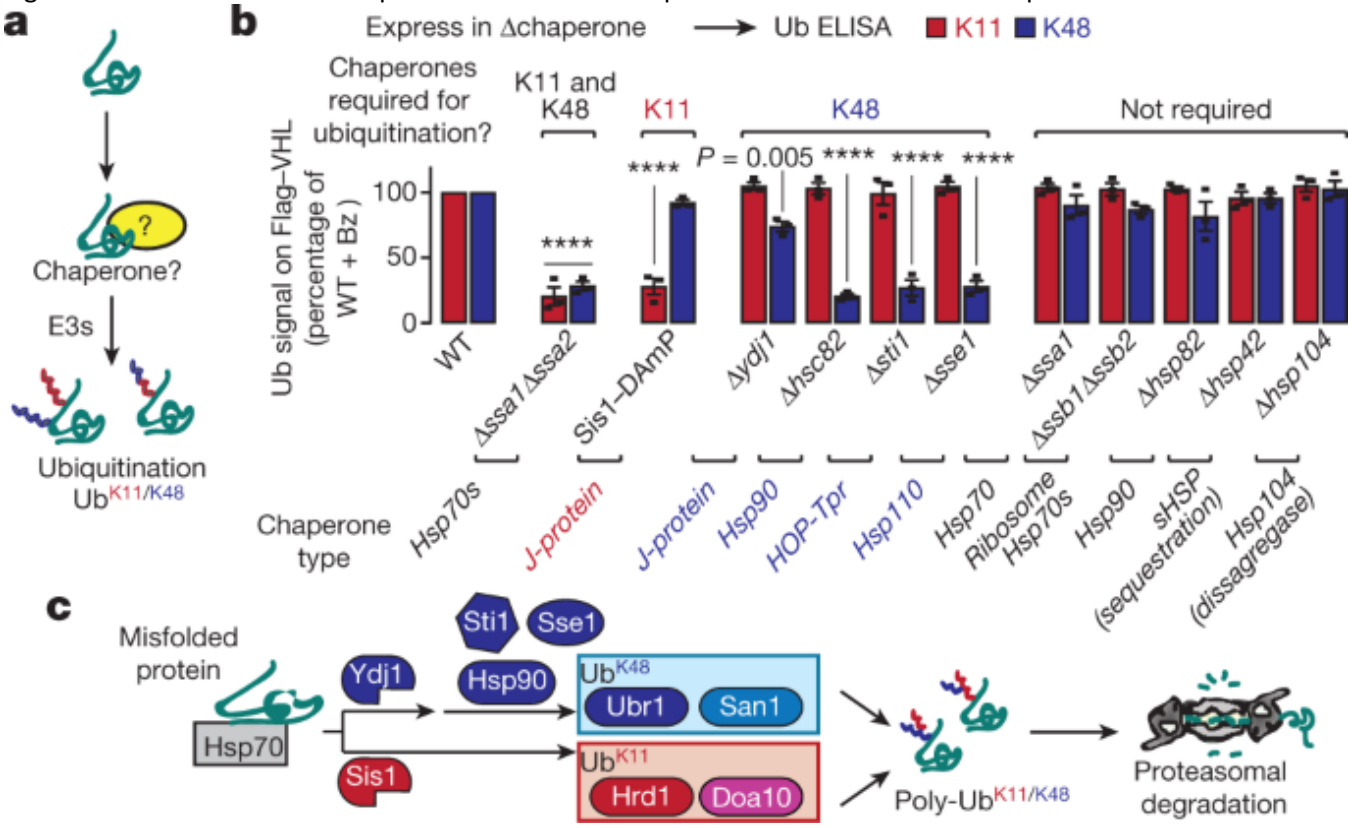

a, Molecular chaperones are involved in the ubiquitination of misfolded proteins by E3 ligases. **b**, Relative amounts of Ub^{K11} and Ub^{K48} present on Flag–VHL in chaperone-deletion strains compared with WT. WT or chaperone-deletion strains expressing Flag–VHL were lysed after 1 h Bz treatment. ELISA for Ub linkages was then performed as described in Extended Data Fig. 3a. Bars represent normalized values from each strain (mean ± s.e.m. from three biologically independent experiments) expressed as a proportion of normalized WT. Strains with statistically significant differences versus WT by one-way ANOVA plus Dunnett's multiple comparisons test are indicated with the adjusted *P* value or with **** for $P < 0.0001$. **c**, Ubiquitination of misfolded proteins through K11 and K48 linkages proceeds through the action of different chaperone pathways.

Binding of Hsp70s to substrates relies on many J-domain proteins, themselves often chaperones that ferry substrates for Hsp70 binding[3,4]. We examined VHL ubiquitination in cells lacking two J-domain proteins, Ydj1 and Sis1, that have been implicated in PQC[7,8,9,11,20,21,22]. Strikingly, each J-domain protein reduced ubiquitination, but in a linkage-specific manner. We found that *Δydj1* cells showed reduced K48 ubiquitination, albeit to a modest degree, probably because Ydj1 is partially redundant with other J-domain co-factors[7]. Depleting cells of the essential Sis1 left K48 ubiquitination unaffected but caused a dramatic loss of K11 ubiquitination. Of note, three other chaperones important for PQC—the Hsp70 nucleotide-exchange factor Sse1 (an Hsp110 chaperone), Hsp90, and Sti1/HOP (which bridges the interaction of Hsp70 with Hsp90)[7,10,11,23]—were all required for K48 ubiquitination but were dispensable for K11 ubiquitination. We conclude that specific chaperone pathways direct PQC substrates to distinct E3 pathways to promote mixed linkage ubiquitination (Fig. 3c). Sis1 cooperates with Hsp70 in promoting Doa10/Hrd1-mediated K11 ubiquitination, whereas the Ydj1/Sse1/Sti1 chaperones cooperate with Hsp70 and Hsp90 for Ubr1/San1-mediated K48 ubiquitination. Requiring two distinct E3 ligases to communicate with distinct chaperone pathways may provide a checkpoint in the triage decision to refold or degrade.

That cytoplasmic misfolded proteins are degraded via a nuclear E3 ligase—San1—was puzzling. In principle, misfolded cytoplasmic proteins might be actively imported into the nucleus for degradation[11,12,20,23]. Alternatively, they might passively diffuse through the nuclear pores, owing to their small size[24]. To directly investigate cytoplasmic-specific and nuclear-specific PQC degradation pathways, we spatially restricted two PQC substrates—VHL and luciferase^{ts}—to the nucleus by using a nuclear localization signal (NLS), or to the cytoplasm by using a nuclear export signal (NES; Fig. 4a). Similar results were obtained for both substrates, corroborating the generality of our conclusions. Treatment with bortezomib showed that both nuclear and cytoplasmic variants are degraded by the UPS (Fig. 4b, c and Extended Data Fig. 6a). NES–GFP–VHL accumulated in cytoplasmic perinuclear puncta, whereas NLS–GFP–VHL accumulated in intranuclear puncta (Fig. 4b). Thus, misfolded proteins are either degraded or form inclusions in the cellular compartment where misfolding occurs.

Fig. 4: Confining misfolded proteins to the nucleus or cytoplasm alters their PQC requirements.

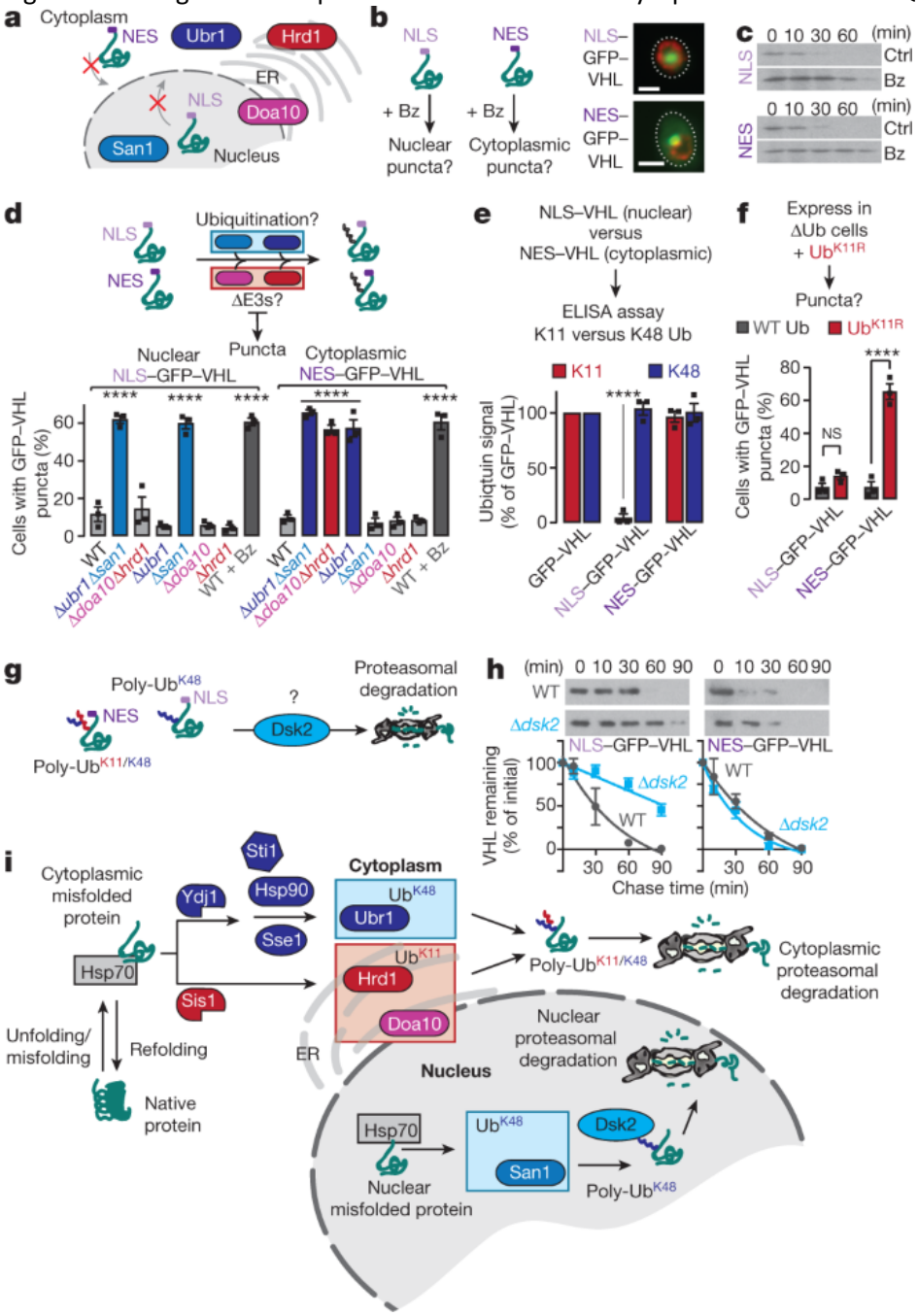

a, **b**, Upon proteasome inhibition, NLS–GFP–VHL (NLS here) and NES–GFP–VHL (NES) accumulate in the nucleus or cytoplasm, respectively. (The red crosses indicate that the proteins are not transported across the nuclear envelope, because of the presence of the NLS or NES.) The locations of the E3s Ubr1, Hrd1, Doa10 and San1 are also shown. **b**, Expression of NLS–GFP–VHL or NES–GFP–VHL in WT cells was shut off in glucose media with 50 μM Bz for 1 h. Cells were immunostained for Nsp1 (a nuclear pore protein; red) and imaged by fluorescence microscopy. Images represent three biologically independent experiments. Scale bars represent 2 μm. **c**, NLS–GFP–VHL and NES–GFP–VHL are cleared by the proteasome. Cycloheximide chase and immunoblot were used to assess the stability of these proteins in WT cells treated with (Bz) or without (Ctrl) 50 μM Bz. Immunoblots represent three biologically independent experiments. **d**, Confining VHL to the nucleus or cytoplasm alters its E3 requirement. The graph shows the percentage of cells with NLS–GFP–VHL or NES–GFP–VHL puncta in deletion strains following 1 h of shut-off. **e**, Nuclear VHL has severely reduced K11–Ub ubiquitin linkages. ELISA performed as in Fig. 2c, but using GFP-multiTrap instead of α-Flag-conjugated plates. **f**, Nuclear VHL clearance is

unaffected by K11–Ub linkages. Experiment performed as in panel **d**, but using cells expressing WT ubiquitin or Ub^{K11R} as the only ubiquitin source. **g**, **h**, Clearance of NLS–GFP–VHL, but not NES–GFP–VHL, requires Dsk2. CHX chase performed as in **c**, but in WT or *Δdsk2* cells. The densitometric quantification in panel **h** is shown relative to $t = 0$ (mean ± s.e.m. from three biologically independent experiments). **i**, Nuclear and cytoplasmic misfolded proteins have distinct clearance requirements. Cytoplasmic misfolded proteins require tagging with both K11–Ub and K48–Ub by chaperones and E3 ligases for proteasomal degradation. In the nucleus, tagging with K48–Ub is sufficient for recognition by Dsk2 and subsequent proteasomal degradation. **d**–**f**, Bars represent mean ± s.e.m. from three biologically independent experiments. Statistically significant differences versus WT (**d**, **f**) or GFP–VHL (**e**) by one-way ANOVA plus Dunnett's multiple comparisons test (**d**, **e**), or two-tailed Student's *t*-test (**f**), are indicated (adjusted *P* value, or ****$P < 0.0001$; NS, $P > 0.05$).

Degradation of cytoplasmic NES–VHL or NES–$luciferase^{ts}$ required the K11 ubiquitin ligases Doa10 and Hrd1, but only the cytoplasmic K48 ligase Ubr1 (Fig. 4d and Extended Data Fig. 6b). Therefore, San1 is dispensable for UPS degradation of strictly cytoplasmic PQC substrates. Surprisingly, the nuclear NLS–GFP–VHL or $luciferase^{ts}$ required only the nuclear K48 ligase, San1, for clearance.

Consistent with their E3 requirements, cytoplasm-restricted misfolded NES-labelled proteins were conjugated to both K11- and K48-linked chains at levels similar to those of their unmodified counterparts. However, nuclear-restricted misfolded NLS-labelled proteins were ubiquitinated only with K48 chains, with the K11 signal reduced to baseline levels (Fig. 4e and Extended Data Fig. 6c). Notably, nuclear misfolded proteins tagged with K48–Ub were efficiently cleared by the proteasome (Fig. 4c, d and Extended Data Fig. 6a). Confirming the distinct role of K11 ubiquitination in nuclear versus cytoplasmic PQC, clearance of NES-tagged misfolded proteins was impaired in Ub^{K11R} cells, whereas degradation of nuclear-restricted PQC substrates was unaffected (Fig. 4f and Extended Data. 6d).

To understand the differences between nuclear and cytoplasmic PQC, we first focused on the ubiquilin Dsk2—a predominantly nuclear[25] shuttling factor that physically ferries K48-ubiquitinated proteins to the proteasome[26]. Strikingly, cells lacking Dsk2 were impaired in clearance of NLS-tagged but not NES-tagged GFP–VHL (Fig. 4g, h). We propose that Dsk2 in the nucleus increases the affinity of K48-only nuclear misfolded proteins for the proteasome.

We examined the role of chaperone circuits in nuclear versus cytoplasmic PQC through functional and proteomic approaches. We found that depletion of Sis1—required for K11 ubiquitination (Fig. 3b)—had no effect on the clearance of NLS-tagged proteins, but, as expected, blocked the clearance of NES-tagged variants (Extended Data Fig. 6d). Interestingly, Hsp90, Sti1, Sse1 and Ydj1 were required only for K48 ubiquitination and clearance of cytoplasmic substrates. Only the Hsp70 proteins—Ssa1 and Ssa2—were required for nuclear PQC.

Mass spectrometry based on stable-isotope labelling by amino acids in cell culture (SILAC) further indicated that PQC of nuclear and cytoplasmic misfolded proteins involves different circuitries. Analysis of immunoprecipitates of NLS-tagged or NES-tagged GFP–VHL (Extended Data Fig. 7 and Extended Table 1) revealed localization-dependent proteostasis interactors (with a $\log_2$(VHL/control ratio) of greater than 0.5). Both nuclear and cytoplasmic PQC substrates shared enrichments in proteasomal subunits and several chaperones, including four Hsp70 proteins. Consistent with their selective requirement for cytoplasmic PQC, Hsp82 and Sis1 specifically associated with NES-tagged VHL. Of note, Cdc48/p97 also selectively associated with NES-tagged VHL, whereas the TRiC/CCT chaperonin selectively associated with NLS-tagged VHL (Extended Data Fig. 7c). The importance of these interactions for PQC will be explored in future studies.

We conclude that the clearance of nuclear and cytoplasmic PQC substrates requires distinct ubiquitin codes, distinct E3 ligases, and distinct chaperone sets. Cytoplasmic PQC requires both K11- and K48-linked ubiquitin,

while nuclear PQC requires only K48-linked ubiquitin. Given that the misfolded protein is the same in both compartments, these distinct requirements are unlikely to relate to the substrate's structural properties, but instead arise from differences in the proteostasis machineries that maintain the nuclear and cytoplasmic proteomes.

Our study opens new perspectives for understanding the circuits and logic of misfolded-protein quality control (Fig. 4i). We define a general PQC path through which specific, non-redundant networks of E3 ligases and chaperones mediate post-translational PQC clearance. Surprisingly, we also uncover marked differences in the pathways of cytoplasmic and nuclear PQC. It is possible that nuclear and cytoplasmic proteasomes differ in composition[27] or concentration[28], affecting their ability to recognize ubiquitinated substrates effectively. It is also possible that K11-linked ubiquitin chains facilitate recognition by another cytoplasmic PQC factor. Intriguingly, Sis1, required for K11 linkages, can act as a sorting factor[9], and is sequestered in protein aggregates[7,8,9,21,29]. Nuclear ubiquilin Dsk2 shuttles K48-linked substrates to nuclear proteasomes, whereas in the cytoplasm, mixed K11/K48 chains enhance the affinity of misfolded proteins for cytoplasmic proteasomes, probably by engaging multiple ubiquitin receptors in the 19S proteasome cap[30].

The distinct ubiquitin linkage requirements for nuclear and cytoplasmic PQC might respond to distinct regulatory and functional rationales for the triage decision between (re-)folding and targeting for degradation. For example, the importance of the UPS in chromatin regulation[31] could sensitize the nuclear proteome to protein misfolding and aggregation[32]—perhaps leading to relaxed ubiquitination requirements for proteasomal recognition. By contrast, the cytosol is a site of active protein biogenesis, assembly and targeting, requiring productive folding intermediates to be safeguarded. Requiring a dual ubiquitin code for cytoplasmic PQC—mediated by distinct E3 ligases and chaperones—would provide a checkpoint to ensure that only non-productive, misfolded proteins are degraded. Of interest, ubiquilin and the PQC E3 ligases identified here are associated with a host of human diseases (Extended Table 2). Dissection of these circuits in normal and diseased states might provide mechanistic clues and open up therapeutic opportunities.

Online content

Any methods, addition porting summaries, source data, statements of data availability and associated accession codes are available at https://doi.org/10.1038/s41586-018-0678-x.

Acknowledgements

We thank K. Li, M. Burlingame and A. L. Burlingame for help with mass spectrometry; R. Andino and F. U. Hartl for critical reading of the manuscript; D. R. Gestaut for sharing the NLS- and NES-tagged plasmids; and all members of the Frydman laboratory for advice. R.S.S. was supported by a Human Frontier Science Program long-term fellowship (LT000695/2015-L). C.M.L. was supported by a National Institutes of Health (NIH) postdoctoral fellowship (1F32CA162919-01A1). This work was supported by an NIH grant (R37GM056433) to J.F. E.M.S. was supported by a postdoctoral fellowship from NIH (F32NS086253).

Additional information

Extended Data Table 2 Human homologues of the ubiquitination machinery characterized here are associated with a range of diseases

Enriched proteins [log,(NLS-VH L/Control) > 0.5)

Fasta headers	log2(Median NLS/Control)
URA3	2.077
CCT5	1.550

SSA2	1.334
SSA4	1.239
MKT1	1.208
TSA1	1.203
TRX2	1.035
CCT8	0.952
ARO1	0.923
MDN1	0.902
RPT6	0.879
CCT7	0.873
TUB1	0.867
CCT3	0.841
GCD6	0.837
TRX1	0.808
BGL2	0.790
VMA2	0.775
AAH1	0.773
NEW1	0.759
RPA135	0.745
SSA1	0.745
YNL134C	0.728
URA?	0.710
PRE10	0.699
EFT1;EFT2	0.688
URA2	0.684
RPT1	0.670
NUG1	0.657
HTS1	0.649
SSB2	0.642
SAM1	0.630
RPB2	0.615
KRE33	0.605
RPN2	0.578
FAS2	0.561
ADE6	0.552
MIS1	0.550
YEF3	0.545
CCT6	0.540
CPA2	0.524
CCT4	0.520
ADE3	0.516
RRP5	0.514
LEU1	0.510
CRM1	0.508
GCN1	0.507
HIS1	0.507
HIS4	0.504
YNL134C	3.229
DBP5	2.501

RKI1	2.494
URA3	2.319
SSA4	2.166
SHM1	1.835
SEC14	1.727
TSA1	1.234
SSA2	1.234
IMD3;IMD2	1.213
SSA1	1.199
TRX2	1.054
GDH1	0.984
BGL2	0.964
TPI1	0.880
RPN3	0.876
CCT5	0.820
CIT1	0.803
TIF4631	0.792
CPA2	0.776
RRP5	0.771
PRE5	0.731
IPP1	0.731
MET17	0.730
DYS1	0.702
SIS1	0.695
TRX1	0.675
MMF1	0.672
ENO2	0.672
PGI1	0.670
RPT6	0.665
PRE9	0.658
HOM6	0.645
HXK2	0.628
ERG10	0.625
BMH1	0.625
UBA1	0.616
PGK1	0.612
HTS1	0.608
YPT52	0.607
SSB2	0.607
URA2	0.598
RPN6	0.597
FPR4	0.592
TKL1	0.578
PRE6	0.571
RNR4	0.561
CDC48	0.558
SDH1	0.535
HSP82	0.526
TUB1	0.520

YPL225W	0.515
TAL1	0.508
LEU1	0.506
GPM1	0.503

Enriched proteins in the NLS–GFP–VHL (left) and NES–GFP–VHL (right) interactomes. Normalized median light/medium (NLS–GFP–VHL) and heavy/medium (NES–GFP–VHL) SILAC ratios from four biologically independent experiments were log2-transformed. Proteins with log2(SILAC ratio) greater than 0.5 were considered as enriched, yielding 49 and 56 proteins for the NLS and NES interactomes, respectively.

Methods

Yeast media, plasmids and strains

Preparation of yeast media, growth, transformations and manipulations were performed according to standard protocols. All E3- and chaperone-deletion yeast strains were derived from the BY4742 wild-type strain. Single deletions were generated by homologous recombination using the *NAT* gene. The Sis1–DAmP strain was also generated in this way. Double deletions were generated with both *NAT* and hygromycin. All strains were checked by polymerase chain reaction (PCR) using at least two sets of primers.

All ubiquitin K-to-R mutant strains—expressing a single, galactose-inducible ubiquitin gene—were gifts from D. Finley (Harvard Univ., MA, USA)[23]. Yeast strains expressing GFP-tagged Doa10 or Hrd1 from their endogenous loci were from the Yeast-GFP Clone Collection (Thermo Fisher Scientific). The *Δdsk2* strain was obtained from the *Saccharomyces* Genome Deletion Project[33]. We acknowledge gifts of pGAL–CPY‡–GFP (R. Hampton, Univ. California San Diego, CA, USA), pADH–Flag–Ubr1 and pGAL–San1–V5His6 (D. Wolf, Univ. Stuttgart, Germany), pFLUC–DM–YFP (F. U. Hartl, Martinsried, Germany), and Ub–M–GFP, Ub–R–GFP, Ub^{G76V}–GFP and GFP–CL1 (N. Dantuma, Karolinska Institute, Stockholm, Sweden)[34]. All other plasmids were constructed using the Gateway cloning technology[35] as described[6].

Galactose shut-off protein expression

Yeast strains transformed with plasmids encoding the galactose-inducible protein of interest were grown overnight in raffinose synthetic medium at 30 °C before dilution to an optical density at 600 nm (OD_{600}) of between 0.05 and 0.1 in galactose synthetic medium. The cells were grown for 4–6 h (OD_{600} 0.6–0.8) to induce expression of the galactose-inducible protein. Expression was shut off by switching the cells to glucose synthetic medium, and the fate of the existing pool of proteins was assessed according to the appropriate downstream application.

Counting puncta-containing cells

Cells were grown as described for galactose shut-off protein expression. Following shut-off, cells were allowed to grow at 30 °C or 37 °C for 1 h in glucose synthetic medium. Note that for WT plus bortezomib conditions, 50 μM bortezomib (LC Laboratories) was dissolved in the glucose synthetic medium before addition. Cells were then fixed for 15 min in 4% paraformaldehyde before mounting onto concanavalin-A-coated coverslips using ProLong^{TM} Diamond Antifade Mountant with DAPI (Thermo Fisher Scientific). Fluorescence was visualized using a Zeiss LSM700 confocal microscope with a ×63 oil-immersion lens. Image analysis was performed by ImageJ software (http://imagej.nih.gov/ij). 300 cells were counted manually for each blinded sample, and the percentage of cells containing GFP-positive puncta was noted. Statistical analysis was performed using one-way ANOVA followed by Dunnett's multiple comparisons test.

Immunofluorescence

Cells were grown and paraformaldehyde fixed as described above. Fixed cells were spheroplasted by incubating for 20–40 min at 30 °C with Zymolyase 100T (Zymo Research) in potassium phosphate buffer (0.1 M potassium phosphate pH 7.5, 1.2 M sorbitol) supplemented with 25 mM DTT and 5 mM EDTA. The resultant spheroplasts were permeabilized with 0.1% (*v/v*) Triton X-100 in potassium phosphate buffer for 10 min. For immunostaining, cells were blocked (potassium phosphate buffer with 1% (*w*/*v*) bovine serum albumin (BSA) for 30 min at room temperature) and incubated overnight at 4 °C with antibodies diluted at the appropriate concentration in potassium phosphate buffer with 0.1% (*w*/*v*) BSA. Antibodies used were against K48–Ub covalently linked to Alexa Fluor 568 (1/100; Abcam catalogue number ab208136), K11–Ub (1/50; EMD Millipore catalogue number MABS107-I) covalently linked to Alexa Fluor 647 NHS Ester (Thermo Fisher Scientific), K11/K48–Ub bispecific antibody (1/500; Genentech) with secondary antibody Cy5-conjugated donkey anti-human (1/1,000; Jackson ImmunoResearch catalogue number 709-175-149), and Nsp1 (1:500, EnCor catalogue number MCA-32D6) with secondary antibody Alexa Fluor 568-conjugated goat anti-mouse (1/1,000; Thermo Fisher Scientific catalogue number A10037) for 1 h at room temperature. Stained cells were mounted onto poly-lysine-coated coverslips using ProLong Diamond Antifade Mountant with DAPI (Thermo Fisher Scientific). Fluorescence was visualized using a Zeiss LSM700 confocal microscope with × 100, numerical aperture 1.4, oil-immersion lens. Raw data collected as *z*-stacks were represented in a single image as maximum-intensity projections (ImageJ).

Cycloheximide chase assay

Cells were grown as described for galactose shut-off protein expression. A first sample with an equivalent OD_{600} of 10 (t = 0) was collected before shut-off. The rest of the culture was shifted to glucose synthetic medium with 50 μg ml^{-1} cycloheximide, and further cells (OD_{600} = 10) were collected 10, 30, 60 and 90 min after the shift. Samples from each time point were pelleted, washed once with 15 mM sodium azide containing 1× Roche cOmplete™ EDTA-free protease-inhibitor tablet (Sigma), snap frozen in liquid nitrogen, and stored at −80 °C until all time points were collected. Proteins were extracted by boiling each sample in an equal volume of 2 × SDS sample buffer (100 mM Tris-HCl pH 6.8, 4% (*w*/*v*) SDS, 20% (*v*/*v*) glycerol, 200 mM DTT, 0.2% (*w*/*v*) bromophenol blue) for 10 min before detection of protein by SDS–PAGE and immunoblotting.

SDS–PAGE and immunoblotting

Protein samples from cell lysates or immunoprecipitates were denatured in SDS sample buffer (95 °C for 5 min) or LDS sample buffer (70 °C for 10 min) before separation by SDS–PAGE. Precision Plus prestained protein standards (Bio-Rad) were used to estimate protein weight. Proteins were transferred onto polyvinylidene fluoride (PVDF) or nitrocellulose membranes (Bio-Rad) and immunoblotted with primary antibodies against GFP (1/1,000; Roche catalogue number 11814460001 or Santa Cruz Biotechnology catalogue number sc-9996), peroxidase anti-peroxidase complex for detection of Protein A in the tandem affinity purification tag (TAP; 1/2,000 to 1/7,500; Sigma catalogue number P1291), glyceraldehyde 3-phosphate dehydrogenase (GAPDH; 1/5,000, Abcam catalogue number ab9485; or 1/10,000, Genetex catalogue number GTX100118), α-tubulin (1/2,500; DSHB Hybridoma Product 12G10; deposited by J. Frankel and E.M. Nelson), Flag (1/1,000; Cell Signaling Technology catalogue number 2368), pan-ubiquitin (1/1,000; Life Sensors catalogue number VU101), K11–Ub (1/100; EMD Millipore catalogue number MABS107-I), K48–Ub (1/1,000; Cell Signaling Technology catalogue number 12805) or K11/K48–Ub bispecific antibody (1/500; Genentech). Specific primary antibodies used are indicated next to the uncropped immunoblot images in Supplementary Fig. 1. For immunoblotting of ubiquitin, samples were separated by SDS–PAGE, transferred to a PVDF membrane and denatured by boiling for 10 min at 95 °C before antibody incubation. Secondary antibodies used were horseradish peroxidase (HRP)-conjugated donkey anti-mouse (1/5,000; Jackson ImmunoResearch catalogue number 715-035-150), donkey anti-rabbit (1/5,000; Jackson ImmunoResearch catalogue number 711-035-152) or donkey anti-human (1/5,000; Jackson ImmunoResearch catalogue number 709-035-149). The HRP signal was detected by incubation with

Pierce ECL Western blotting substrate (Thermo Fisher Scientific) and exposure to GeneMate Blue Ultra Film (BioExpress). Immunoblots shown are representative of three independent experiments.

Immunoprecipitation of E3 ligases

To test for co-immunoprecipitation of E3 ligases, we transfected pADH–Flag–Ubr1 or pGAL–San1–V5His6 plasmids into yeast strains from the yeast-GFP collection (expressing GFP-tagged Doa10 or Hrd1 from the endogenous loci). Each strain was grown overnight in raffinose synthetic media at 30 °C before dilution to an OD_{600} of between 0.05 and 0.1 in galactose synthetic media. The cells were grown for 24 h to induce expression of the galactose-inducible San1–V5His6, diluted back to OD_{600} = 0.1, and then grown for another 4–6 h (OD_{600} 0.6–0.8). For consistency between experimental conditions, the same protocol was followed for cells expressing Flag–Ubr1 from the alcohol dehydrogenase (ADH) promoter, even though this does not require galactose for expression. Cells were pelleted and washed once with 15 mM sodium azide supplemented with 1× Roche cOmplete™ EDTA-free protease-inhibitor tablet (Sigma) and 50 mM 2-chloroacetamide, to inhibit proteases and deubiquitinases, respectively. Pellets were resuspended in an equal volume of lysis buffer (50 mM Tris-HCl pH 7.5, 150 mM NaCl, 2 mM EDTA, 1 mM phenylmethane sulfonyl fluoride (PMSF) Roche cOmplete™ EDTA-free protease-inhibitor tablet (Sigma), 50 mM 2-chloroacetamide, 10 µM PR-619 (Sigma)) and frozen drop-wise in liquid nitrogen by passing through a 20.5-gauge syringe. Frozen samples were lysed by cryogrinding in a Retsch MM-301 (five cycles, 30 Hz, for 3 min per cycle) and proteins solubilized by adding Triton X-100 (1% *v*/*v* final concentration). Lysates were clarified (16,000*g* for 30 min at 4 °C) and quantified for total protein by bicinchonic acid (BCA) assay. We incubated 2 mg of lysate with anti-GFP rabbit IgG conjugated to protein G dynabeads (Thermo Fisher Scientific) for 2 h at 4 °C to immunoprecipitate the GFP-tagged protein complexes, which were then eluted from the beads by heating for 30 min at 70 °C in non-reducing LDS sample buffer (Thermo Fisher Scientific). The bead-free samples were reduced with DTT (50 mM final concentration, 10 min at 70 °C) before SDS–PAGE analysis.

Immunoprecipitation of ubiquitinated VHL

For immunoprecipitation of ubiquitinated Flag–VHL, yeast strains were grown as described for galactose shut-off protein expression. Following shut-off in glucose synthetic medium supplemented with 50 µM Bz for 1 h at 30 °C, cells were pelleted and snap frozen in liquid nitrogen. All subsequent steps were performed at 4 °C or on ice. Pellets were resuspended in an equal volume of urea lysis buffer (50 mM Tris-HCl pH 7.5, 8 M urea, 150 mM NaCl, 2 mM EDTA, 1 mM PMSF, Roche cOmplete™ EDTA-free protease inhibitor tablet (Sigma), 50 mM chloroacetamide, 10 µM PR-619 (Sigma)) and lysed by bead beating (five cycles at 1 min each, with 1 min on ice in between cycles). Following dilution tenfold in Triton immunoprecipitation buffer (same composition as urea lysis buffer, but with 1% *v*/*v* Triton X-100 instead of 8 M urea), lysates were clarified (16,000*g* for 30 min at 4 °C) and quantified for total protein by BCA assay. We incubated 2 mg of lysates with Flag-M2 magnetic beads (Sigma) for 2 h at 4 °C to immunoprecipitate the Flag-tagged protein, which was then eluted from the beads by heating for 30 min at 70 °C in non-reducing LDS sample buffer (Thermo Fisher Scientific), to avoid co-elution of the Flag antibody. The bead-free samples were reduced with DTT (50 mM final concentration, 10 min at 70 °C) before SDS–PAGE analysis.

The same protocol was used for denaturing immunoprecipitation of ubiquitinated GFP–VHL, but with addition of 1% *w*/*v* SDS in lysis and immunoprecipitation buffers, and incubation with GFP-TRAP_MA magnetic beads (ChromoTek) instead of Flag-M2 magnetic beads.

For double-immunoprecipitation experiments, 10 mg of cell lysate was incubated with Flag-M2 magnetic beads for 2 h at 4 °C and eluted from the beads by competition with 3× Flag peptide (Apex Bio). The resultant eluate was subsequently incubated with an antibody against K48–Ub (1/500; Cell Signaling Technologies catalogue number 4289) or K11–Ub (1/50; EMD Millipore catalogue number MABS107-I) covalently conjugated using

bis(sulfosuccinimidyl)suberate (BS^3) to protein G dynabeads (Thermo Fisher Scientific) overnight at 4 °C. The bead-bound fraction ('eluate') was eluted by heating for 10 min at 70 °C in non-reducing LDS sample buffer, and analysed alongside the unbound fraction ('flow-through') by SDS–PAGE.

Ubiquitin linkage ELISA

For quantification of K11–Ub and K48–Ub linkages on Flag–VHL, cell lysates were prepared as described for immunoprecipitation of ubiquitinated Flag–VHL. We added 200 µg of lysate protein to each well of an anti-Flag-M2-coated 96-well plate and then incubated the plate for 2 h. All incubation steps were performed at room temperature with gentle shaking. Four wells were used for each technical replicate (two replicates per strain per experiment). After washing four times with Triton immunoprecipitation buffer to remove unbound protein, each well was incubated for 1 h with rabbit antibodies against one of GFP (1/1,000; Cell Signaling Technology catalogue number 2956), Flag (1/1,000; Cell Signaling Technology catalogue number 2368), K11–Ub (1/50; EMD Millipore catalogue number MABS107-I), or K48–Ub (1/500; Cell Signaling Technology catalogue number 4289) diluted in 100 µl tris-buffered saline/Tween-20 (TBS-T) buffer with 0.1% BSA. After another four washes, each well was incubated for 1 h with HRP-conjugated donkey anti-rabbit antibody (1/2,000; Jackson ImmunoResearch catalogue number 711-035-152) diluted in 100 µl TBS-T with 0.1% BSA, washed another four times with Tween immunoprecipitation buffer, and incubated for 30 min with 100 µl Pierce tetramethylbenzidine (TMB) substrate (Thermo Fisher Scientific) followed by 100 µl 0.16 M sulfuric acid to stop the reaction. Absorbance was measured at 450 nm.

To calculate the K11–Ub or K48–Ub signal for each strain, we subtracted the raw absorbance readings of the negative control (GFP) signal, and then divided by the Flag signal to account for variations in total Flag–VHL levels. These K11–Ub or K48–Ub signals were then expressed as a proportion of the K11–Ub or K48–Ub signal in the WT strain to allow direct comparison between strains. Bars represent means ± s.e.m. from three individual experiments.

The same protocol was followed for quantification of linkages on GFP-tagged proteins, except with the use of GFP-multiTrap 96-well plates (ChromoTek) instead of Flag-M2-coated plates, and using the GFP and Flag signals as positive and negative controls, respectively.

SILAC mass spectrometry of VHL immunoprecipitates

WT yeast cells transfected with one of NLS–GFP–VHL, NES–GFP–VHL or Flag–VHL were grown overnight at 30 °C in raffinose-synthetic media supplemented with light Lys0 (Cambridge Isotope Laboratories catalogue number ULM-8766-PK), heavy Lys8 (Cambridge Isotope Laboratories catalogue number CNLM-291-H-1) or medium Lys4 (Cambridge Isotope Laboratories catalogue number DLM-2640-PK), respectively. Cells were diluted to an OD_{600} of between 0.05 and 0.1 in galactose synthetic medium supplemented with the appropriate lysine isotopes and grown for 4–5 h (OD_{600} 0.6–0.8) to induce expression of the galactose-inducible protein. Expression was shut off by switching the cells to glucose synthetic medium supplemented with the appropriate lysine isotope. Pelleted cells were lysed by cryogrinding as described in the 'Immunoprecipitation of E3 ligases' section above. Then, 1.5 mg of protein (as quantified by BCA assay) from each of the NLS–GFP–VHL, NES–GFP–VHL and Flag–VHL lysates were mixed before immunoprecipitation using GFP-TRAP_MA magnetic beads (ChromoTek) according to the manufacturer's protocol. After three washes with Triton immunoprecipitation buffer, the beads were washed twice with 50 mM Tris-HCl pH 8 supplemented with 20 mM $CaCl_2$. On-bead trypsin digestion and peptide clean-up were performed using the in-StageTip method[36]. Peptides were analysed on a Q Exactive Plus Orbitrap (Thermo Fisher Scientific) connected to a NanoAcquity high-performance liquid-chromatography system (Waters). An EASY-Spray PepMap rapid-separation liquid-chromatography column (C18, 3 µm, 75 µm × 15 cm; Thermo Fisher Scientific) was used to resolve peptides with a binary solvent system (0.1% formic acid in water as mobile phase A, 0.1% formic acid in acetonitrile as mobile phase B). The Q Exactive Plus was run

on a linear 60-min gradient from 2% to 30% phase B at a flow rate of 300 nl min^{-1}. Both precursor and fragment ions were analysed in the flow-through (FT) mode at a mass resolution of 70,000 and 17,500, respectively. After a survey scan, the ten most intense precursor ions were selected for subsequent fragmentation by higher-energy collisional dissociation.

Raw data from four biological replicates were processed using MaxQuant37 (http://www.coxdocs.org/doku.php?id=maxquant:start, version 1.6.2.3) and searched against the *Saccharomyces* Genome Database (https://downloads.yeastgenome.org/sequence/S288C_reference/orf_protein; downloaded in January 2015) with common contaminant entries. The default MaxQuant parameters for a triple SILAC experiment were used, with the exception of 'Re-quantify', which was enabled.

The proteinGroups.txt file was filtered to exclude contaminants, reverse hits, hits 'only identified by site', and hits for which only one peptide was identified. The normalized SILAC ratios were used to generate median fold-change values per protein. Proteins with a $\log_2$(light/medium) or $\log_2$(heavy/medium) value of more than 0.5 were counted as 'enriched' in NLS–VHL or NES–VHL interactomes, respectively. Enriched proteins from each interactome were subjected to pathway analysis to search for enriched Gene Ontology (GO) terms, Kyoto Encyclopedia of Genes and Genomes (KEGG) pathways and PFAM protein domains in either interactome using the STRING database[38] (http://string-db.org, version 10.5).

Reporting summary

Further information on experimental design is available in the Nature Research Reporting Summary linked to this paper.

Data availability

The data sets generated and/or analysed during this study are available from the corresponding author on reasonable request. The mass spectrometry proteomics data have been deposited to the ProteomeXchange Consortium (http://proteomecentral.proteomexchange.org) via the PRIDE partner repository with the data identifier PXD010660. Uncropped images of all immunoblots shown in this study are in Supplementary Fig. 1.

References

1. Chiti, F. & Dobson, C. M. Protein misfolding, amyloid formation, and human disease: a summary of progress over the last decade. *Annu. Rev. Biochem*. **86**, 27–68 (2017).
2. Balch, W. E., Morimoto, R. I., Dillin, A. & Kelly, J. W. Adapting proteostasis for disease intervention. *Science* **319**, 916–919 (2008).
3. Sontag, E. M., Samant, R. S. & Frydman, J. Mechanisms and functions of spatial protein quality control. *Annu. Rev. Biochem*. **86**, 97–122 (2017).
4. Balchin, D., Hayer-Hartl, M. & Hartl, F. U. *In vivo* aspects of protein folding and quality control. *Science* **353**, aac4354 (2016).
5. Kwon, Y. T. & Ciechanover, A. The ubiquitin code in the ubiquitin-proteasome system and autophagy. *Trends Biochem. Sci*. **42**, 873–886 (2017).
6. Kaganovich, D., Kopito, R. & Frydman, J. Misfolded proteins partition between two distinct quality control compartments. *Nature* **454**, 1088–1095 (2008).
7. Escusa-Toret, S., Vonk, W. I. & Frydman, J. Spatial sequestration of misfolded proteins by a dynamic chaperone pathway enhances cellular fitness during stress. *Nat. Cell Biol*. **15**, 1231–1243 (2013).

8. Malinovska, L., Kroschwald, S., Munder, M. C., Richter, D. & Alberti, S. Molecular chaperones and stress-inducible protein-sorting factors coordinate the spatiotemporal distribution of protein aggregates. *Mol. Biol. Cell* **23**, 3041–3056 (2012).
9. Park, S. H. et al. PolyQ proteins interfere with nuclear degradation of cytosolic proteins by sequestering the Sis1p chaperone. *Cell* **154**, 134–145 (2013).
10. McClellan, A. J., Scott, M. D. & Frydman, J. Folding and quality control of the VHL tumor suppressor proceed through distinct chaperone pathways. *Cell* **121**, 739–748 (2005).
11. Heck, J. W., Cheung, S. K. & Hampton, R. Y. Cytoplasmic protein quality control degradation mediated by parallel actions of the E3 ubiquitin ligases Ubr1 and San1. *Proc. Natl Acad. Sci. USA* **107**, 1106–1111 (2010).
12. Prasad, R., Kawaguchi, S. & Ng, D. T. A nucleus-based quality control mechanism for cytosolic proteins. *Mol. Biol. Cell* **21**, 2117–2127 (2010).
13. Deng, M. & Hochstrasser, M. Spatially regulated ubiquitin ligation by an ER/nuclear membrane ligase. *Nature* **443**, 827–831 (2006).
14. Swanson, R., Locher, M. & Hochstrasser, M. A conserved ubiquitin ligase of the nuclear envelope/endoplasmic reticulum that functions in both ER-associated and Matalpha2 repressor degradation. *Genes Dev*. **15**, 2660–2674 (2001).
15. Jin, L., Williamson, A., Banerjee, S., Philipp, I. & Rape, M. Mechanism of ubiquitin-chain formation by the human anaphase-promoting complex. *Cell* **133**, 653–665 (2008).
16. Xu, P. et al. Quantitative proteomics reveals the function of unconventional ubiquitin chains in proteasomal degradation. *Cell* **137**, 133–145 (2009).
17. Yau, R. & Rape, M. The increasing complexity of the ubiquitin code. *Nat. Cell Biol*. **18**, 579–586 (2016).
18. Yau, R. G. et al. Assembly and function of heterotypic ubiquitin chains in cell-cycle and protein quality control. *Cell* **171**, 918–933 (2017).
19. Spence, J., Sadis, S., Haas, A. L. & Finley, D. A ubiquitin mutant with specific defects in DNA repair and multiubiquitination. *Mol. Cell. Biol*. **15**, 1265–1273 (1995)
20. Prasad, R., Xu, C. & Ng, D. T. W. Hsp40/70/110 chaperones adapt nuclear protein quality control to serve cytosolic clients. *J. Cell Biol*. **217**, 2019–2032 (2018).
21. Summers, D. W., Wolfe, K. J., Ren, H. Y. & Cyr, D. M. The type II Hsp40 Sis1 cooperates with Hsp70 and the E3 ligase Ubr1 to promote degradation of terminally misfolded cytosolic protein. *PLoS One* **8**, e52099 (2013).
22. Shiber, A., Breuer, W., Brandeis, M. & Ravid, T. Ubiquitin conjugation triggers misfolded protein sequestration into quality control foci when Hsp70 chaperone levels are limiting. *Mol. Biol. Cell* **24**, 2076–2087 (2013).
23. Guerriero, C. J., Weiberth, K. F. & Brodsky, J. L. Hsp70 targets a cytoplasmic quality control substrate to the San1p ubiquitin ligase. *J. Biol. Chem*. **288**, 18506–18520 (2013).
24. Amm, I. & Wolf, D. H. Molecular mass as a determinant for nuclear San1-dependent targeting of misfolded cytosolic proteins to proteasomal degradation. *FEBS Lett*. **590**, 1765–1775 (2016).
25. Biggins, S., Ivanovska, I. & Rose, M. D. Yeast ubiquitin-like genes are involved in duplication of the microtubule organizing center. *J. Cell Biol*. **133**, 1331–1346 (1996).
26. Tsuchiya, H. et al. *In vivo* ubiquitin linkage-type analysis reveals that the Cdc48-Rad23/Dsk2 axis contributes to K48-linked chain specificity of the proteasome. *Mol. Cell* **66**, 488–502 (2017).
27. Fabre, B. et al. Subcellular distribution and dynamics of active proteasome complexes unraveled by a workflow combining *in vivo* complex cross-linking and quantitative proteomics. *Mol. Cell. Proteomics* **12**, 687–699 (2013).
28. Russell, S. J., Steger, K. A. & Johnston, S. A. Subcellular localization, stoichiometry, and protein levels of 26 S proteasome subunits in yeast. *J. Biol. Chem*. **274**, 21943–21952 (1999).

29. Miller, S. B. et al. Compartment-specific aggregases direct distinct nuclear and cytoplasmic aggregate deposition. *EMBO J*. **34**, 778–797 (2015).
30. Chen, X. et al. Structures of Rpn1 T1:Rad23 and hRpn13:hPLIC2 reveal distinct binding mechanisms between substrate receptors and shuttle factors of the proteasome. *Structure* **24**, 1257–1270 (2016).
31. Ben Yehuda, A. et al. Ubiquitin accumulation on disease associated protein aggregates is correlated with nuclear ubiquitin depletion, histone de-ubiquitination and impaired DNA damage response. *PLoS One* **12**, e0169054 (2017).
32. Zhong, Y. et al. Nuclear export of misfolded SOD1 mediated by a normally buried NES-like sequence reduces proteotoxicity in the nucleus. *eLife* **6**, e23759 (2017).
33. Winzeler, E. A. et al. Functional characterization of the *S. cerevisiae* genome by gene deletion and parallel analysis. *Science* **285**, 901–906 (1999).
34. Dantuma, N. P., Lindsten, K., Glas, R., Jellne, M. & Masucci, M. G. Short-lived green fluorescent proteins for quantifying ubiquitin/proteasome-dependent proteolysis in living cells. *Nat. Biotechnol*. **18**, 538–543 (2000).
35. Alberti, S., Gitler, A. D. & Lindquist, S. A suite of Gateway cloning vectors for high-throughput genetic analysis in *Saccharomyces cerevisiae*. *Yeast* **24**, 913–919 (2007).
36. Kulak, N. A., Pichler, G., Paron, I., Nagaraj, N. & Mann, M. Minimal, encapsulated proteomic-sample processing applied to copy-number estimation in eukaryotic cells. *Nat. Methods* **11**, 319–324 (2014).
37. Cox, J. & Mann, M. MaxQuant enables high peptide identification rates, individualized p.p.b.-range mass accuracies and proteome-wide protein quantification. *Nat. Biotechnol*. **26**, 1367–1372 (2008).
38. Szklarczyk, D. et al. The STRING database in 2017: quality-controlled protein-protein association networks, made broadly accessible. *Nucleic Acids Res*. **45** (D1), D362–D368 (2017).
39. Hassink, G. et al. TEB4 is a C4HC3 RING finger-containing ubiquitin ligase of the endoplasmic reticulum. *Biochem. J*. **388**, 647–655 (2005).
40. Loregger, A. et al. A MARCH6 and IDOL E3 ubiquitin ligase circuit uncouples cholesterol synthesis from lipoprotein uptake in hepatocytes. *Mol. Cell. Biol*. **36**, 285–294 (2015).
41. Stevenson, J., Luu, W., Kristiana, I. & Brown, A. J. Squalene mono-oxygenase, a key enzyme in cholesterol synthesis, is stabilized by unsaturated fatty acids. *Biochem. J*. **461**, 435–442 (2014).
42. Zelcer, N. et al. The E3 ubiquitin ligase MARCH6 degrades squalene monooxygenase and affects 3-hydroxy-3-methyl-glutaryl coenzyme A reductase and the cholesterol synthesis pathway. *Mol. Cell. Biol*. **34**, 1262–1270 (2014).
43. Nomura, J. et al. Neuroprotection by endoplasmic reticulum stress-induced HRD1 and chaperones: possible therapeutic targets for Alzheimer's and Parkinson's disease. *Med. Sci*. **4**, E14 (2016).
44. Joshi, V., Upadhyay, A., Kumar, A. & Mishra, A. Gp78 E3 ubiquitin ligase: essential functions and contributions in proteostasis. *Front. Cell. Neurosci*. **11**, 259 (2017).
45. Zenker, M. et al. Deficiency of UBR1, a ubiquitin ligase of the N-end rule pathway, causes pancreatic dysfunction, malformations and mental retardation (Johanson-Blizzard syndrome). *Nat. Genet*. **37**, 1345–1350 (2005); corridgendum 38, 265 (2006).
46. George, A. J., Hoffiz, Y. C., Charles, A. J., Zhu, Y. & Mabb, A. M. A comprehensive atlas of E3 ubiquitin ligase mutations in neurological disorders. *Front. Genet*. **9**, 29 (2018).
47. Mezghrani, A. et al. A destructive interaction mechanism accounts for dominant-negative effects of misfolded mutants of voltage-gated calcium channels. *J. Neurosci*. **28**, 4501–4511 (2008).
48. Manganas, L. N. et al. Episodic ataxia type-1 mutations in the Kv1.1 potassium channel display distinct folding and intracellular trafficking properties. *J. Biol. Chem*. **276**, 49427–49434 (2001).
49. Mittal, S., Dubey, D., Yamakawa, K. & Ganesh, S. Lafora disease proteins malin and laforin are recruited to aggresomes in response to proteasomal impairment. *Hum. Mol. Genet*. **16**, 753–762 (2007).

50. Atkin, T. A., Brandon, N. J. & Kittler, J. T. Disrupted in schizophrenia 1 forms pathological aggresomes that disrupt its function in intracellular transport. *Hum. Mol. Genet*. **21**, 2017–2028 (2012).
51. Crider, A., Ahmed, A. O. & Pillai, A. Altered expression of endoplasmic reticulum stress-related genes in the middle frontal cortex of subjects with autism spectrum disorder. *Mol. Neuropsychiatry* **3**, 85–91 (2017).
52. De Jaco, A., Comoletti, D., King, C. C. & Taylor, P. Trafficking of cholinesterases and neuroligins mutant proteins. An association with autism. *Chem. Biol. Interact*. **175**, 349–351 (2008).
53. De Jaco, A. et al. A mutation linked with autism reveals a common mechanism of endoplasmic reticulum retention for the alpha,beta-hydrolase fold protein family. *J. Biol. Chem*. **281**, 9667–9676 (2006).
54. De Jaco, A. et al. Neuroligin trafficking deficiencies arising from mutations in the alpha/beta-hydrolase fold protein family. *J. Biol. Chem*. **285**, 28674–28682 (2010).
55. Fujita, E. et al. Autism spectrum disorder is related to endoplasmic reticulum stress induced by mutations in the synaptic cell adhesion molecule, CADM1. *Cell Death Dis*. **1**, e47 (2010).
56. Ulbrich, L. et al. Autism-associated R451C mutation in neuroligin3 leads to activation of the unfolded protein response in a PC12 Tet-On inducible system. *Biochem. J*. **473**, 423–434 (2016).
57. El Ayadi, A., Stieren, E. S., Barral, J. M. & Boehning, D. Ubiquilin-1 and protein quality control in Alzheimer disease. *Prion* **7**, 164–169 (2013).
58. Marín, I. The ubiquilin gene family: evolutionary patterns and functional insights. *BMC Evol. Biol*. **14**, 63 (2014).
59. Safren, N. et al. Ubiquilin-1 overexpression increases the lifespan and delays accumulation of Huntingtin aggregates in the R6/2 mouse model of Huntington's disease. *PLoS One* **9**, e87513 (2014).
60. Natunen, T. et al. Relationship between ubiquilin-1 and BACE1 in human Alzheimer's disease and APdE9 transgenic mouse brain and cell-based models. *Neurobiol. Dis*. **85**, 187–205 (2016).
61. Deng, H. X. et al. Mutations in UBQLN2 cause dominant X-linked juvenile and adult-onset ALS and ALS/dementia. *Nature* **477**, 211–215 (2011).
62. Osaka, M., Ito, D. & Suzuki, N. Disturbance of proteasomal and autophagic protein degradation pathways by amyotrophic lateral sclerosis-linked mutations in ubiquilin 2. *Biochem. Biophys. Res. Commun*. **472**, 324–331 (2016).
63. Teyssou, E. et al. Novel UBQLN2 mutations linked to amyotrophic lateral sclerosis and atypical hereditary spastic paraplegia phenotype through defective HSP70-mediated proteolysis. *Neurobiol Aging* **58**, 239e11–239e220 (2017).
64. Zeng, L. et al. Differential recruitment of UBQLN2 to nuclear inclusions in the polyglutamine diseases HD and SCA3. *Neurobiol. Dis*. **82**, 281–288 (2015).
65. Hjerpe, R. et al. UBQLN2 mediates autophagy-independent protein aggregate clearance by the proteasome. *Cell* **166**, 935–949 (2016).

Extended data figures and tables

Extended Data Fig. 1 E3 ligases work in optimal combinations to clear misfolded proteins.

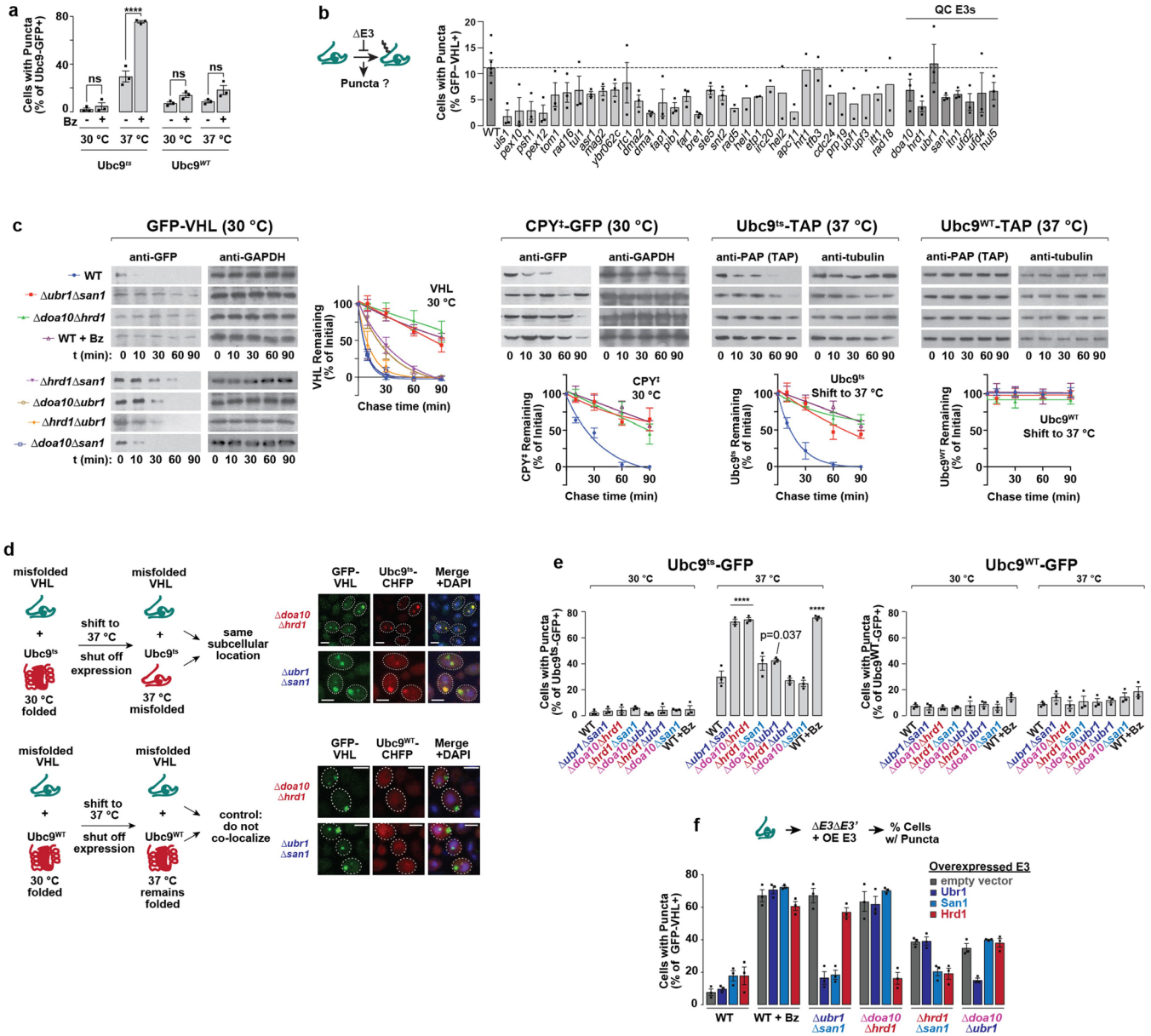

a, Assay for puncta formation distinguishes between misfolded versus natively folded proteins. WT cells expressing natively folded Ubc9WT–GFP or temperature-sensitive Ubc9ts–GFP from a galactose-inducible promoter for 4–6 h at 30 °C were shifted to glucose-containing medium for 1 h at 30 °C or 37 °C to shut off expression. Cells were fixed and imaged by fluorescence microscopy. 300 cells were counted per condition, and the percentage of cells with GFP-positive puncta is shown (means ± s.e.m. from three biologically independent experiments). Only cells expressing Ubc9ts–GFP showed a statistically significant change in the percentage of puncta-positive cells compared with WT (two-tailed Student's t-test, ****P < 0.0001; ns, not significant). b, Deletion of individual E3 ligases does not increase puncta formation. Experiment performed as in panel a, but using strains with endogenous deletions of the genes shown on the x-axis. E3 ligases that have previously been implicated in PQC (as shown in Fig. 1d) are grouped to the right (QC, quality control). Bars represent mean ± s.e.m. from three biologically independent experiments, with the exception of rad5, hel1, etp1, irc20, hel2, apc11, hrt1, tfb3, cdc24, prp19, upf1, upf3, itt1 and rad18, where bars represent the mean from two

biologically independent experiments, as well as WT, where bars represent the mean ± s.e.m. from seven biologically independent experiments. No strains showed statistically significant differences compared with WT by one-way ANOVA followed by Dunnett's multiple comparisons test. c, Deleting certain pairs of E3 ligases increases the stability of misfolded proteins. CHX chase was followed by immunoblot to assess the stability of GFP–VHL, CPY‡–GFP, Ubc9ts–TAP or Ubc9WT–TAP in E3 double-deletion strains. For the WT + Bz condition, 50 μM Bz was added to the glucose-containing medium 10 min before CHX treatment. Graphs represent densitometric quantification of bands relative to t = 0 (mean ± s.e.m. from three biologically independent experiments). d, Multiple misfolded proteins are sequestered in the same subcellular location. Δubr1Δsan1 or Δdoa10Δhrd1 strains co-expressing VHL with temperature-sensitive Ubc9ts (top) or natively folded Ubc9WT (bottom) from galactose-inducible promoters for 5–6 h at 30 °C were shifted to glucose-containing medium for 1 h at 37 °C. Fluorescence microscopy images are representative of at least 100 cells from each of three biologically independent experiments. e, Deletion of certain pairs of E3s increases puncta formation. Experiment performed as in panel a, but in strains with endogenous deletions of pairs of E3 genes. Each right-hand panel shows experiments in which cells were shifted to 37 °C for the 1 h of galactose shut-off. Bars represent means ± s.e.m. from three biologically independent experiments. Strains for which statistically significant differences were observed by one-way ANOVA followed by Dunnett's multiple comparisons test compared with WT are indicated with the adjusted P value or with **** for $P < 0.0001$. f, Overexpressing a single E3 ligase does not compensate for the loss of others. Ubr1, San1 or Hrd1 were overexpressed alongside GFP–VHL in the indicated strains. The rest of the experiment was performed as in a. Bars represent means ± s.e.m. from three biologically independent experiments.

Extended Data Fig. 2 San1 forms a complex with Doa10 but not with Hrd1.

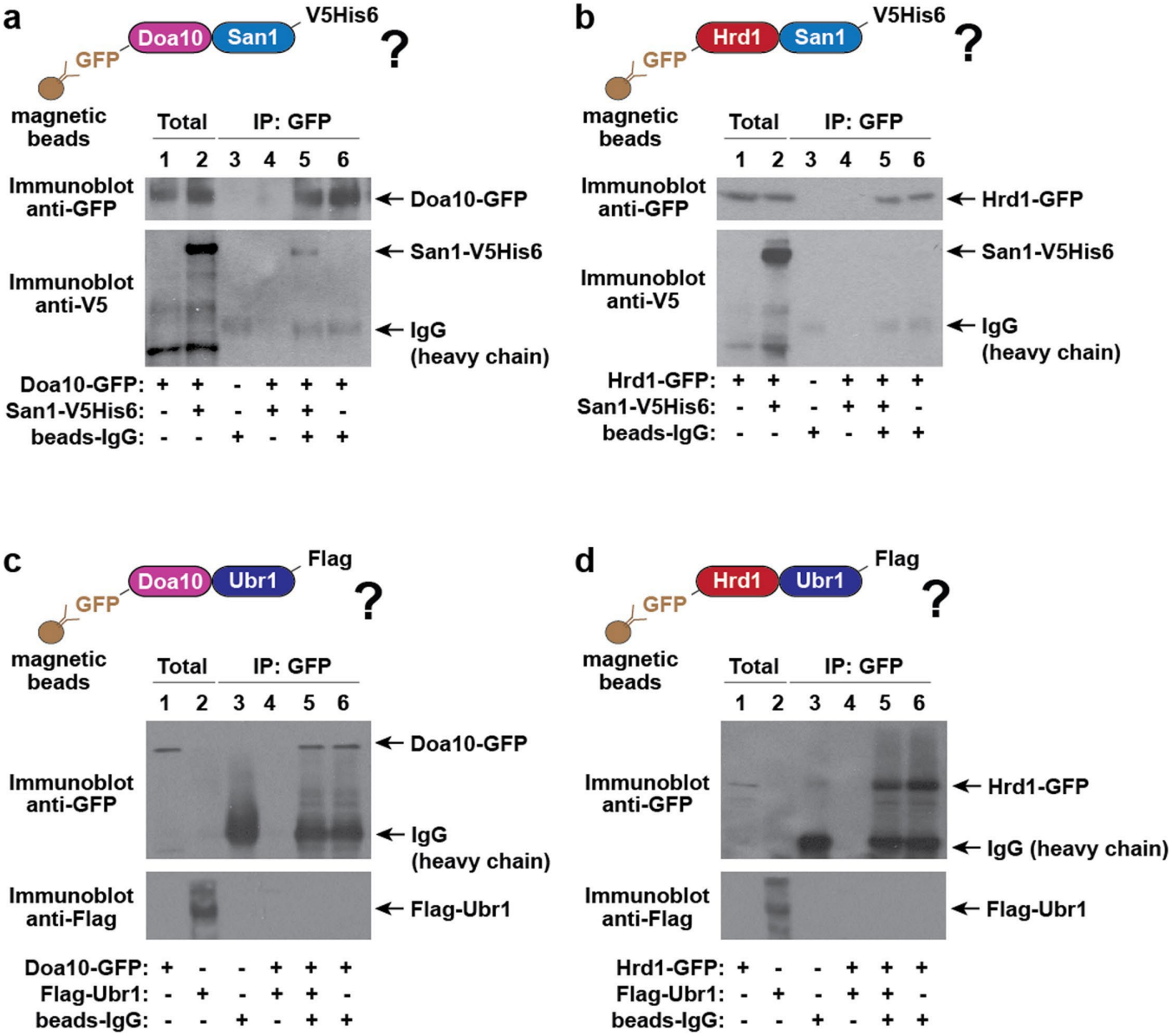

a, b, San1–V5His6 co-immunoprecipitates with Doa10–GFP but not with Hrd1–GFP. Yeast cells co-expressing Doa10–GFP (a) or Hrd1–GFP (b) from their endogenous promoters with San1–V5His6 from a galactose-inducible promoter for 16 h were shifted to 37 °C for 1 h, and immediately lysed by cryo-grinding. Native complexes were immunoprecipitated with GFP-Trap-MA nanobodies before immunoblotting with the indicated antibodies. Immunoblots are representative of three biologically independent experiments. c, d, Flag–Ubr1 does not co-immunoprecipitate with Doa10–GFP or Hrd1–GFP. The experiment was performed as in panel a and b, but with cells expressing Flag–Ubr1 (from the constitutive ADH promoter) instead of San1–V5His6. Immunoblots are representative of three biologically independent experiments.

Extended Data Fig. 3 K48–Ub and K11–Ub linkages are reduced in Δubr1Δsan1 and Δdoa10Δhrd1 strains, respectively.

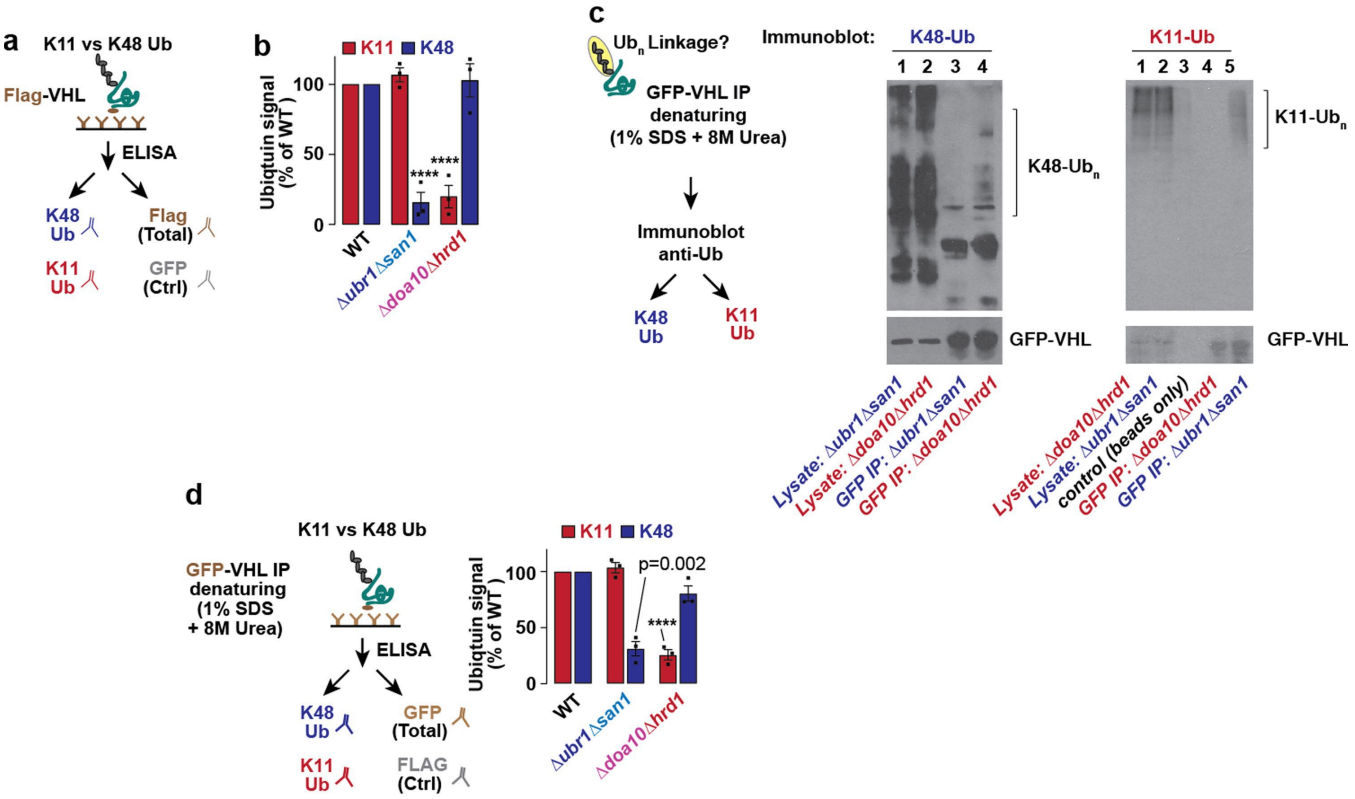

a, Diagram showing the Ub-linkage ELISA used to quantify Ub linkages. Flag–VHL from a yeast lysate was immunoprecipitated in an anti-Flag-conjugated 96-well plate (using four wells per sample), and incubated with antibodies against GFP (negative control), Flag, K11–Ub, or K48–Ub. Following incubation with a secondary antibody (anti-rabbit-HRP), the strength of each signal was detected by electrochemiluminescence at 450 nm. To quantify the K11–Ub or K48–Ub linkages on Flag–VHL, we subtracted the anti-K11 or anti-K48 signal from the negative control (anti-GFP) and normalized to the total Flag–VHL signal for each sample. b, Ub-linkage ELISA confirms that K48–Ub and K11–Ub linkages are reduced on Flag–VHL in Δubr1Δsan1 and Δdoa10Δhrd1 strains, respectively. WT or E3 double-deletion strains expressing Flag-VHL at 30 °C for 4–6 h were lysed after 1 h Bz treatment, also at 30 °C. Ub-linkage ELISA was then performed as described in a. Bars represent Flag-normalized values from each strain (mean ± s.e.m. from three biologically independent experiments), expressed as a proportion of the Flag-normalized WT values. Strains with statistically significant differences compared with WT by one-way ANOVA followed by Dunnett's multiple comparisons test are indicated (****$P < 0.001$). c, GFP–VHL denaturing immunoprecipitation (1% SDS + 8 M urea) followed by immunoblot for K48–Ub or K11–Ub in WT or E3 double-deletion strains. Immunoblots are representative of three independent experiments. d, Relative amounts of K11–Ub and K48–Ub linkages present on GFP–VHL in Δubr1Δsan1 or Δdoa10Δhrd1 strains compared with WT. WT or E3 double-deletion strains expressing GFP–VHL at 30 °C for 5–6 h were lysed in denaturing conditions (1% SDS + 8 M urea) after 1 h Bz treatment, also at 30 °C. Ub-linkage ELISA was then performed using GFP-multiTrap plates. Bars represent GFP-normalized values from each strain (means ± s.e.m. from three biologically independent experiments) expressed as a proportion of the GFP-normalized WT values. Strains for which statistically significant differences were observed by one-way ANOVA followed by Dunnett's multiple comparisons test compared with WT are indicated with the adjusted P value, or with **** for $P < 0.0001$.

Extended Data Fig. 4 K11–Ub linkages are not necessary for proteasomal degradation of all cytoplasmic substrates.

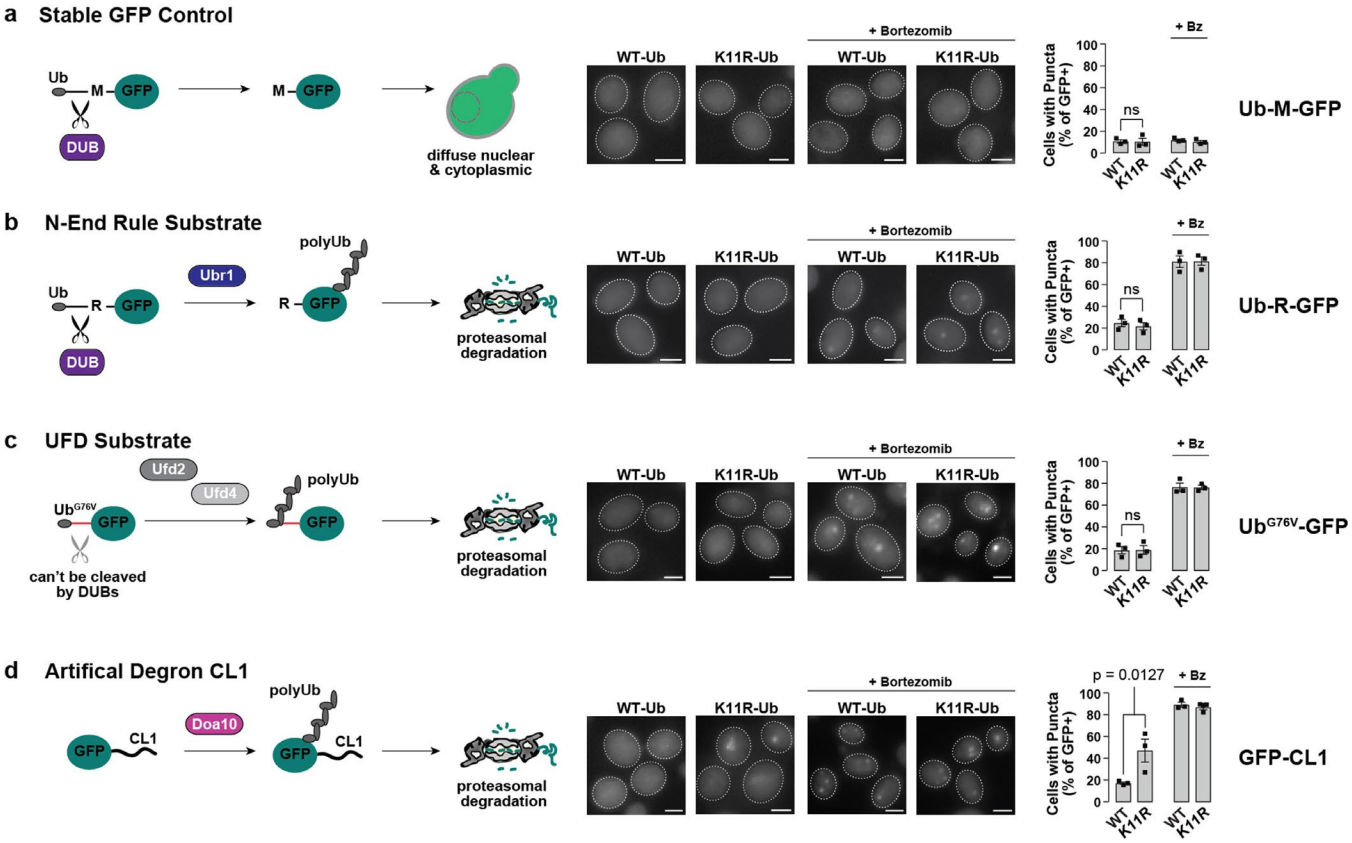

a–d, WT or UbK11R cells expressing stable Ub-M-GFP (a), the N-end-rule substrate Ub-R-GFP (b), the ubiquitin fusion degradation (UFD) substrate UbG76V–GFP (c) or GFP fused to the artificial degron CL1 (d) from galactose-inducible promoters for 4–6 h at 30 °C were shifted to glucose-containing medium for 1 h at 30 °C or 37 °C to shut off expression. Cells were fixed and imaged by fluorescence microscopy. 300 cells were counted per condition, and the percentage of cells with GFP-positive puncta is shown (mean ± s.e.m. from three biologically independent experiments). There was a statistically significant increase in puncta compared with WT when GFP-CL1 (which contains a short amphipathic CL1 helix that could mimic a partially unfolded protein) was expressed in UbK11R cells, as judged by two-tailed Student's t-test ($P = 0.0127$). The differences for all other substrates were not significant (ns, $P > 0.05$). DUB, deubiquitinating enzyme, which cleaves Ub from Ub-M-GFP or Ub-R-GFP.

Extended Data Fig. 5 Misfolded VHL is modified with branched K11/K48 ubiquitin chains.

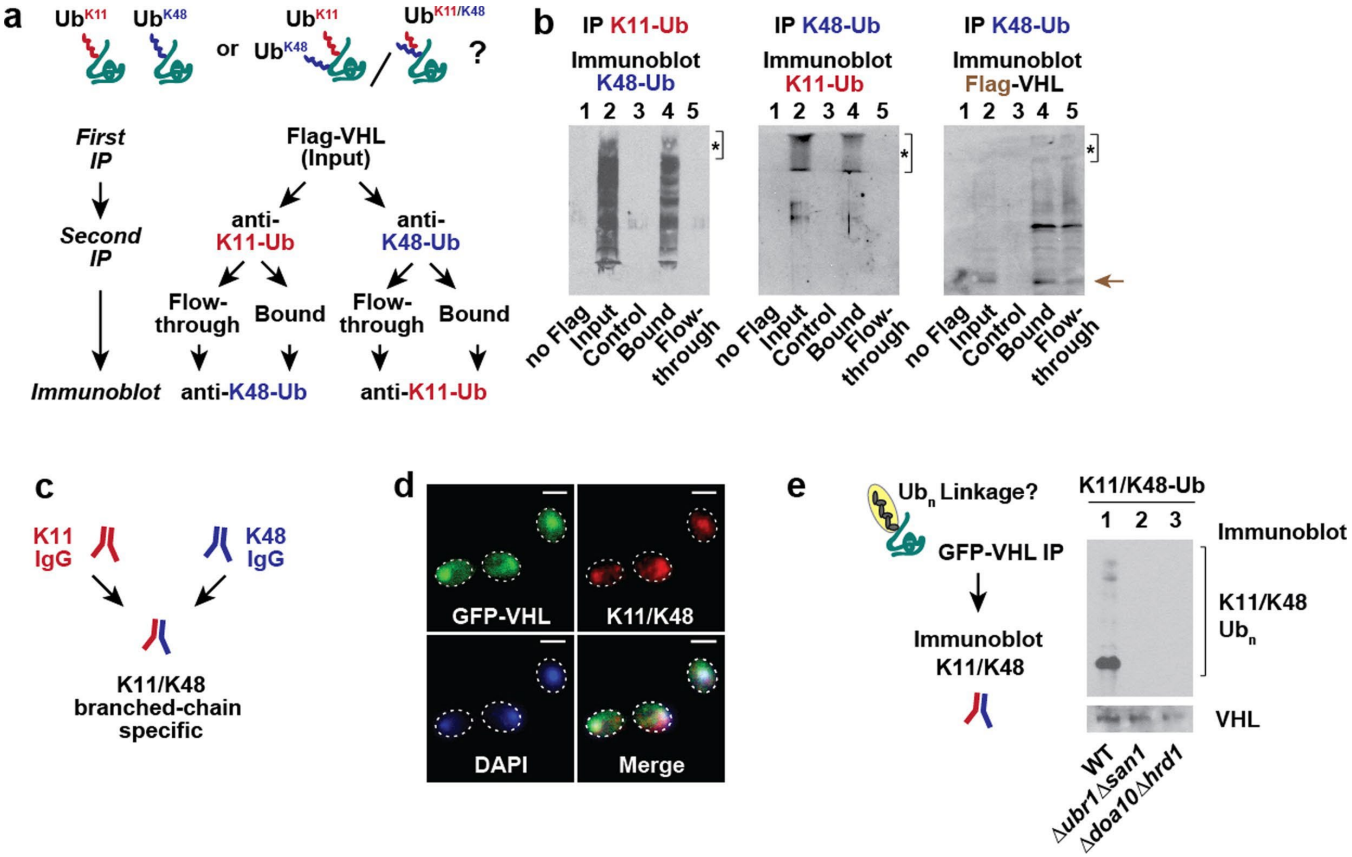

a, b, Both K11–Ub and K48–Ub linkages are present on the same VHL molecule. a, This experiment was designed to determine whether both K48–Ub and K11–Ub linkages are present in the same VHL population. Sequential immunoprecipitation was carried out, first with anti-Flag antibody, then with an anti-K11–Ub or anti-K48–Ub antibody. The resulting negative control ('no Flag', with mock Flag plus K11 or K48 immunoprecipitation with lysate from cells expressing GFP–VHL instead of Flag–VHL), bead control ('Control', with no K11–Ub or K48–Ub antibody), 'Bound' and 'Flow-through', in addition to samples with just the first Flag immunoprecipitation (Input), were subjected to SDS–PAGE and immunoblotted for the presence of the other Ub linkage (b).Immunoblots representative of three biologically independent experiments are shown. The arrow indicates the size of un-ubiquitinated Flag–VHL. The asterisks indicate proteins in the stacking gel that did not enter the resolving gel. c, This bispecific anti-K11/K48–Ub antibody was designed to bind ubiquitin chains with K11 and K48 linkages branching off the same ubiquitin moiety. d, Misfolded VHL co-localizes with K11/K48–Ub chains. WT cells expressing GFP–VHL from a galactose-inducible promoter for 4–6 h at 30 °C were shifted to glucose-containing medium with 50 μM bortezomib for 1 h to shut off expression. Cells were fixed, spheroplasted and detergent permeabilized before immunostaining with an antibody designed to recognize ubiquitin that had K11 and K48 linkages emanating from the same moiety (K11/K48). Confocal fluorescence microscopy images are representative of at least 100 cells from each of three biologically independent experiments. Scale bars represent 2 μm. e, VHL is modified with branched K11/K48–Ub chains. GFP–VHL denaturing immunoprecipitation was followed by immunoblot for K11/K48–Ub or GFP (VHL) in WT or E3 double-deletion strains. Immunoblots representative of three biologically independent experiments are shown.

Extended Data Fig. 6 Nuclear and cytoplasmic proteins require different PQC pathways for clearance.

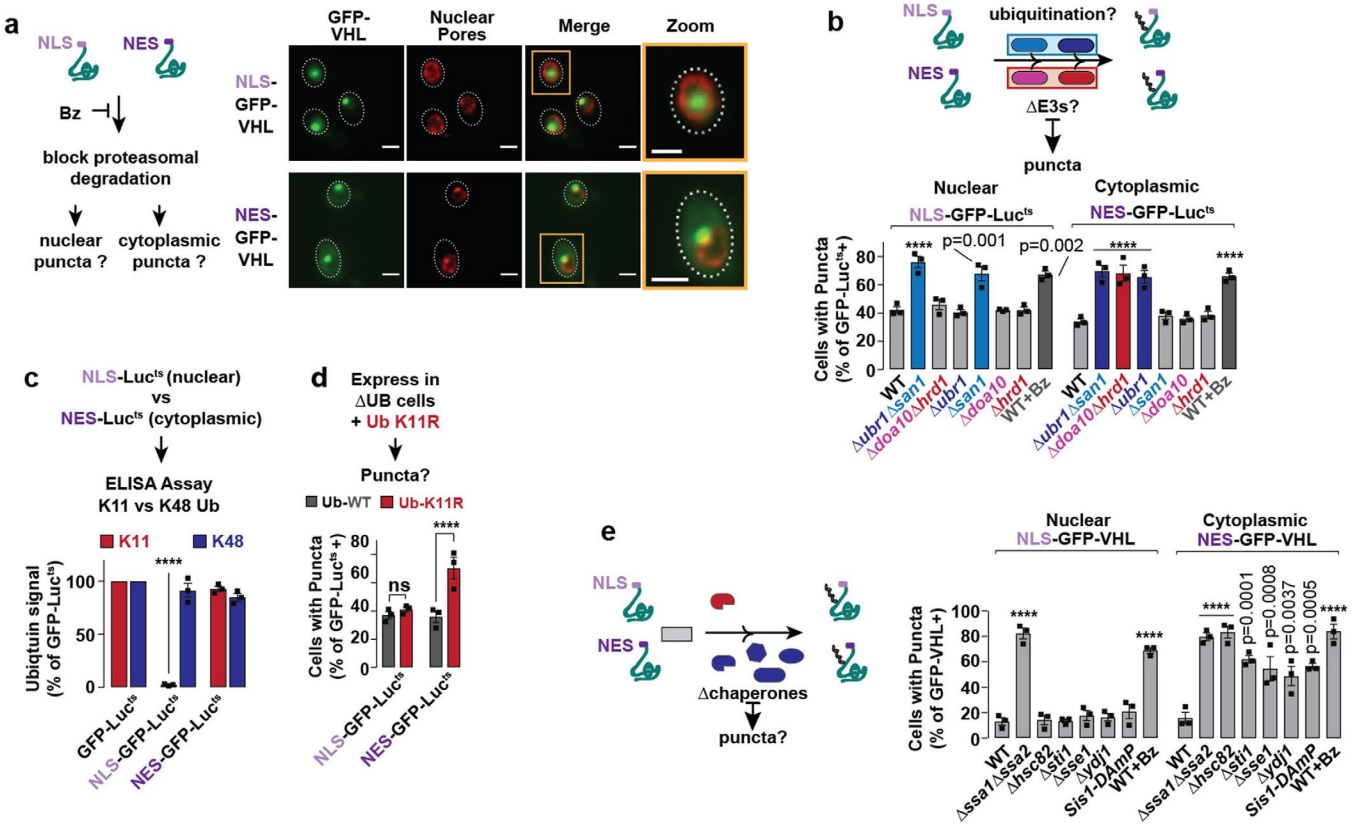

a, NLS–GFP–VHL and NES–GFP–VHL form a single punctum in the nucleus or cytoplasm, respectively, upon proteasome inhibition. WT cells expressing NLS–GFP–VHL or NES–GFP–VHL from a galactose-inducible promoter for 4–6 h at 30 °C were shifted to glucose-containing medium with 50 µM Bz for 1 h at 30 °C to shut off GFP–VHL expression. Fixed and spheroplasted cells were immunostained for the nuclear pore complex protein Nsp1 (red) before imaging by fluorescence microscopy. Representative cells from three biologically independent repeats are shown. b–d, Misfolded luciferasets (Lucts) confined to the nucleus can be cleared by San1-mediated K48-linked ubiquitination. b, The increase in the percentage of cells containing puncta of NLS–GFP–Lucts and NES–GFP–Lucts across the E3 single- and double-deletion strains is similar to the pattern observed with NLS–GFP–VHL and NES–GFP–VHL in Fig. 4. Shown is the percentage of cells (mean ± s.e.m. from three biologically independent experiments, each with n = 300) containing NLS–GFP–Lucts or NES–GFP–Lucts puncta in WT, single- or double-deletion strains after 4–6 h expression of the protein at 30 °C followed by 1 h shut-off at 37 °C. Strains for which statistically significant differences were observed by one-way ANOVA followed by Dunnett's multiple comparisons test compared with WT are indicated with the adjusted P value, or with **** for $P < 0.0001$. c, Misfolded nuclear Lucts has severely reduced K11–Ub linkages (****$P < 0.0001$ by one-way ANOVA followed by Dunnett's multiple comparisons test). Ubiquitin-linkage ELISA was performed on lysates of WT yeast expressing NLS-, NES- or unaltered GFP–Lucts at 37 °C as described in Extended Data Fig. 2c, but in GFP-multiTrap 96-well plates instead of anti-Flag-conjugated 96-well plates. Anti-Flag was used instead of anti-GFP as the ELISA negative control. Bars represent means ± s.e.m. from three biologically independent experiments. d, Misfolded luciferasets confined to the nucleus does not require K11–Ub linkages for clearance. The experiment was performed as in panel b, but with yeast strains expressing WT or mutant K11R–Ub as their sole source of ubiquitin. 300 cells were counted per condition, and the percentages of cells with GFP-positive puncta are shown in (means ± s.e.m. from three biologically independent experiments). Only NES–GFP–Lucts had a statistically significant change in puncta-positive cells in the K11R strain when compared with WT (one-way ANOVA followed by Dunnett's multiple comparisons test; ****$P < 0.0001$; ns = $P > 0.05$). e, VHL confined to the nucleus (NLS) or cytoplasm (NES) requires different chaperones for clearance. The experiment was performed as

in panel b, but with the indicated chaperone-deletion strains. Bars represent means ± s.e.m. from three biologically independent experiments. Strains for which statistically significant differences were observed compared with WT by one-way ANOVA followed by Dunnett's multiple comparisons test are indicated with the adjusted P value, or with **** for P < 0.0001.

Extended Data Fig. 7 Mass spectrometry of the VHL interactome identifies distinct PQC circuitries for nuclear and cytoplasmic VHL.

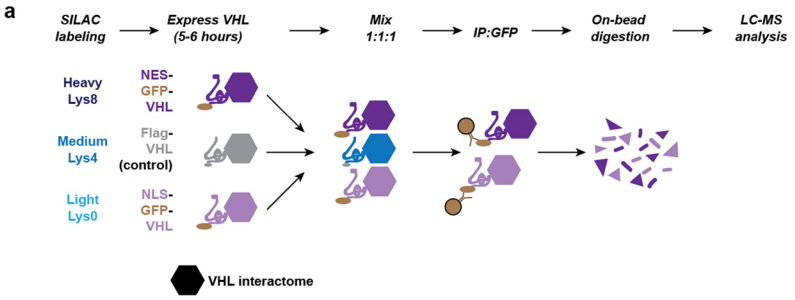

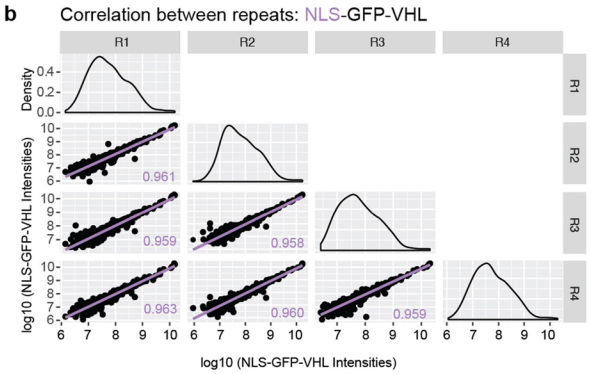

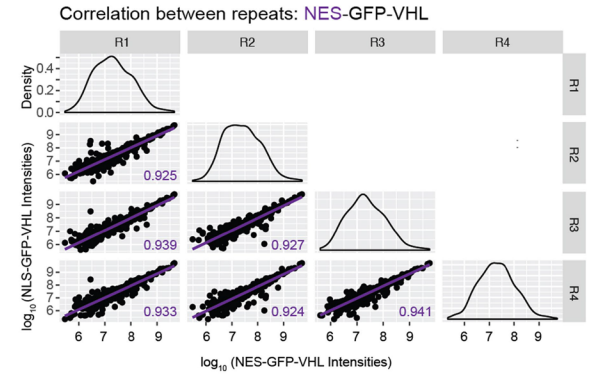

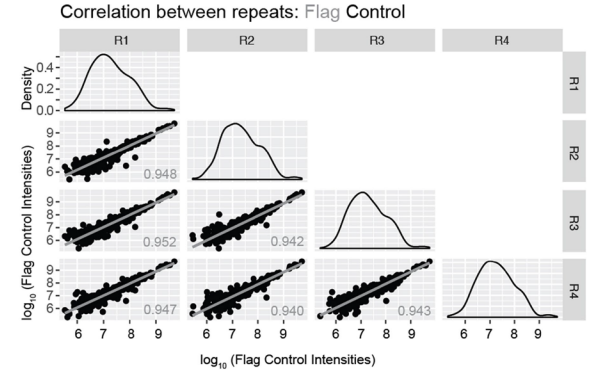

c **Enriched PQC proteins [$\log_2$(VHL/Control) > 0.5]**

	NLS-GFP-VHL	NES-GFP-VHL
Proteasome		
20S core particle	Pre10	
		Pre5
		Pre6
		Pre9
19S regulatory particle	Rpt6	Rpt6
	Rpt1	
	Rpn2	
		Rpn3
		Rpn6
Chaperones		
Hsp70 family	Ssa1	Ssa1
	Ssa2	Ssa2
	Ssa4	Ssa4
	Ssb2	Ssb2
Hsp90 family		Hsp82
Hsp40 family		Sis1
TRiC/CCT	Cct5	Cct5
	Cct3	
	Cct4	
	Cct6	
	Cct7	
	Cct8	
Thioredoxins	Trx1	Trx1
	Trx2	Trx2
	Tsa1	Tsa1
14-3-3		Bmh1
Degradation machinery		Uba1
		Cdc48
		Crm1

d **Selected enriched PQC pathways (adjusted p < 0.05)**

	Adjusted p-value	
	NLS-GFP-VHL	NES-GFP-VHL
GO-Biological Process		
Proteasome assembly	0.0189	0.0286
Protein folding	n.s.	0.0121
GO-Molecular Function		
Unfolded protein binding	0.0076	0.0047
GO-Cellular Component		
Chaperonin-containing T-complex	2.87E-09	n.s.
KEGG Pathways		
Proteasome	0.00401	6.27E-06
PFAM Protein Domains		
TCP-1/cpn60 chaperonin family	2.49E-06	n.s.
Hsp70 protein	0.00229	0.00787

a, Triple SILAC-base mass spectrometry of VHL immunoprecipitates. WT yeast cells transfected with one of NLS–GFP–VHL, NES–GFP–VHL or Flag–VHL were grown overnight at 30 °C in raffinose-synthetic media supplemented with light Lys0, heavy Lys8 or medium Lys4, respectively. Growth of VHL was induced in galactose for 4–5 h before shut off in glucose for 90 min. Next, 1.5 mg of protein from each of the three lysed samples were mixed before immunoprecipitation using GFP-TRAP_MA magnetic bead on-bead restriction digestion and peptide clean-up. Peptides were identified using liquid-chromatography/mass-spectrometry analysis before analysis using MaxQuant. b, Strong correlation between the four biological repeats (R1–R4). Raw intensities for light (NLS–GFP–VHL; top), heavy (NES–GFP–VHL; middle) and medium (VHL–Flag control, bottom) were log10-transformed and plotted as scatterplot matrices. The Pearson correlation coefficient for each pairwise comparison is indicated, and the density distribution of intensities within each repeat is shown in the diagonal axis of the matrices. c, Enriched PQC proteins in NLS–GFP–VHL and NES–GFP–VHL interactomes. Normalized median light/medium (NLS–GFP–VHL) and heavy/medium (NES–GFP–VHL) SILAC ratios were log2-transformed. Proteins with log2(SILAC ratio) of greater than 0.5 were considered as enriched, yielding 49 and 56 proteins for the NLS and NES interactomes, respectively. Enriched proteins known to play a role in PQC are shown. Both nuclear and cytoplasmic VHL share enrichments in proteasomal subunits, the Hsp70 chaperones Ssa1, Ssa2, Ssa4 and Ssb2, and the thioredoxins Trx1, Trx2 and Tsa1 (previously implicated in misfolded-protein management). All enriched proteins are shown in Extended Data Table 1. d, Enriched PQC pathways in NLS–GFP–VHL and NES–GFP–VHL interactomes. The enriched proteins from each interactome (median values from four biologically independent experiments) were subjected to pathway analysis to search for enriched GO terms, KEGG pathways and PFAM protein domains in either interactome using the STRING database. Selected enriched PQC pathways are shown ($P < 0.05$ using Fisher's exact test followed by Benjamini–Hochberg multiple testing correction).

Extended data table 2 | human homologues of the ubiquitination machinery characterized here are associated with a range of diseases

Yeast gene	Human orthologue	Associated Diseases	PQC in disease pathology?
Doa10	MARCH6/TEB4	Cri-du-chat syndrome (same chromosomal region)[39] ; Lipidogenesis imbalance [40-42]	-
Hrd1	HRD1	Alzheimer 's Disease Parkinson's Disease	[43] (Review)
	Gp78/AMFR	Cancer Cystic fibrosis ALS Parkinson's Disease Huntington's Disease Prion disorders	[44] (Review)
Ubr1	UBR1	Johanson-Blizzard Syndrome[45]	[45]
	UBR4	Episod ic Ataxia Type 8 [46]	Unclear (yes for related Types 1 & 2) [47,48]
	UBR5	Adult Myoclonal Epilepsy	[46]Unclear (yes for related Lafora Myoclonal Epilepsy) [49]
	UBR7	Autism Spectrum Disorder [46]	[50-56]
San1	No clear human orthologue	-	-
Dsk2	UBQLN1	Alzheimer's Disease Huntington's Disease	[51,58] (Reviews), [59,60]

	UBQLN2	ALS Frontotemporal Dementia Huntington's Disease	61-65

Literature-based evidence for disease pathology being directly related to PQC is indicated in the last column, where applicable. References cited are[39-65].